International Journal of Earth Sciences (2021) 110:1293–1319
https://doi.org/10.1007/s00531-021-02016-w

ORIGINAL PAPER

Metabasic rocks from the Variscan Schwarzwald (SW Germany): metamorphic evolution and igneous protoliths

Rainer Altherr[1] · Stefan Hepp[1,2] · Hans Klein[3,4] · Michael Hanel[1]

Received: 16 July 2020 / Accepted: 26 February 2021 / Published online: 22 March 2021

Abstract

In the Variscan Schwarzwald metabasic rocks form small bodies included within anatectic plagioclase-biotite gneisses. Many metabasites first underwent an eclogite-facies metamorphism at about 2.0 GPa and 670–700 °C, resulting in the assemblage garnet + omphacite + rutile + quartz ± epidote ± amphibole ± kyanite. Since these eclogites are nearly free of an OH-bearing phase, they underwent almost complete dehydration during subduction, suggesting formation along an average to warm top-of-the-slab geotherm of 10–13 °C/km. The age of the Variscan high-*P*/high-*T* metamorphism is > 333 Ma. After partial exhumation from ~ 65 to ~ 15 km depth, the eclogites were overprinted under increasing activity of H_2O by a number of retrograde reactions. The degree of this overprint under amphibolite-facies conditions (0.4–0.5 GPa/675–690 °C) was very different. Up to now, only retrograde eclogites have been found, but some samples still contain omphacite. Kyanite is at least partially transformed to aggregates of plagioclase + spinel ± corundum ± sapphirine. On the other hand, there are amphibolites that are extensively recrystallized and show the assemblage amphibole + plagioclase + ilmenite/titanite ± biotite ± quartz ± sulphides. The last relic phase that can be found in such otherwise completely recrystallized amphibolites is rutile. After the amphibolite-facies metamorphism at ~ 333 Ma, the metabasites underwent a number of low-temperature transformations, such as sericitization of plagioclase, chloritization of amphibole, and formation of prehnite. The intimate association of metabasite bodies with gneisses of dominantly meta-greywacke compositions suggests derivation from an active plate margin. This view is corroborated by bulk-rock geochemical data. Excluding elements that were mobile during metamorphism (Cs, Rb, Ba, K, Pb, Sr, U), the concentrations of the remaining elements in most of the metabasites are compatible with a derivation from island-arc tholeiites, back-arc basin basalts or calc-alkaline basalts. Only some samples have MORB precursor rocks.

Keywords Retrograde eclogite · Amphibolite · Basaltic protolith · Metamorphic evolution · Schwarzwald · Germany

Introduction

Many collisional belts contain metabasic rocks that were metamorphosed under variable *P*–*T* conditions. Although such rocks may quantitatively be of minor importance, they often play a substantial role in the interpretation of orogenic belts. Their metamorphic parageneses and textures may throw light on their geodynamic evolution before and during continental collision. Furthermore, their bulk-rock chemistry may give valuable information on the tectonic environment in which their igneous precursor rocks were generated (island or continental arc versus rift, plume or mid-ocean ridge). Such information may help to get a better idea of the tectonostratigraphic evolution of an orogenic belt. However, due to manifold metasomatic processes at variable *P*–*T* conditions, bulk-rock chemical compositions

✉ Rainer Altherr
rainer.altherr@geow.uni-heidelberg.de

[1] Institute of Earth Science, Heidelberg University, Im Neuenheimer Feld 234–236, 69120 Heidelberg, Germany

[2] Present Address: Hirschbergstraße 16/1, 88400 Biberach, Germany

[3] Institut für Geo- und Umweltwissenschaften, Mineralogie–Petrologie, University of Freiburg, Albertstraße 23b, 79104 Freiburg, Germany

[4] Present Address: Auf dem Buck 4, 79761 Waldshut-Tiengen, Germany

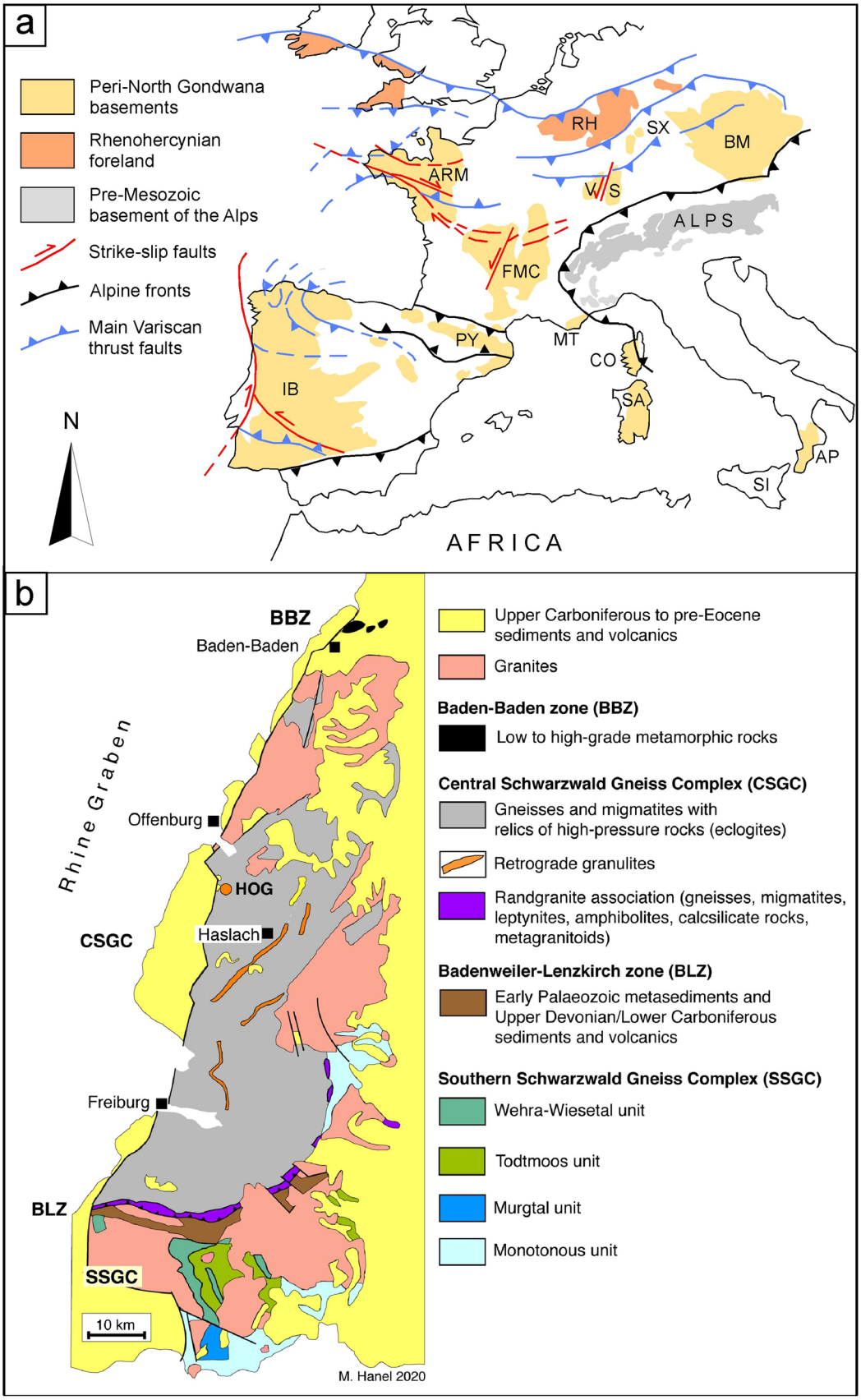
a
Peri-North Gondwana basements
Rhenohercynian foreland
Pre-Mesozoic basement of the Alps
Strike-slip faults
Alpine fronts
Main Variscan thrust faults
N
RH
SX
BM
ARM
W
S
ALPS
FMC
PY
MT
CO
IB
SA
AP
SI
AFRICA
b
BBZ
Baden-Baden
Rhine Graben
Offenburg
HOG
Haslach
CSGC
Freiburg
BLZ
SSGC
10 km
M. Hanel 2020
Upper Carboniferous to pre-Eocene sediments and volcanics
Granites
Baden-Baden zone (BBZ)
Low to high-grade metamorphic rocks
Central Schwarzwald Gneiss Complex (CSGC)
Gneisses and migmatites with relics of high-pressure rocks (eclogites)
Retrograde granulites
Randgranite association (gneisses, migmatites, leptynites, amphibolites, calcsilicate rocks, metagranitoids)
Badenweiler-Lenzkirch zone (BLZ)
Early Palaeozoic metasediments and Upper Devonian/Lower Carboniferous sediments and volcanics
Southern Schwarzwald Gneiss Complex (SSGC)
Wehra-Wiesetal unit
Todtmoos unit
Murgtal unit
Monotonous unit

◂**Fig. 1** **a** Sketch map showing outcrops of the European Variscides. *AP* Apulian Massif, *ARM* Armorican Massif, *BM* Bohemian Massif, *CO* Corsica, *FMC* French Massif Central, *IB* Iberian Massif, *MT* Mauretanian Massif, *PY* Pyrenees, *RH* Rhenohercynian Zone, *S* Schwarzwald, *SA* Sardinia, *SI* Sicily, *SX* Saxothuringian Zone, *V* Vosges Mts. **b** Geological sketch map of the Schwarzwald. Unlike the SSGC that is differentiated into four metamorphic units, the CSGC is undifferentiated, with the exception of the retrograde granulites. HOG stands for the mafic metagranulites from Hohengeroldseck Castle

may change significantly during orogenesis and may blur the primary igneous character of a metabasic rock. Hence, the major problem is to disentangle the effects of various metasomatic alteration events in order to understand and reconstruct the chemical changes that affected these rocks.

In the Moldanubian Zone of the European Variscides (Kossmat 1927) polymetamorphic metabasites are widespread (e.g. Fluck 1974; Klein and Wimmernauer 1984; Finger and Steyrer 1995; Faryad et al. 2013; Benmamar et al. 2020; de Hoÿm et al. 2020; Lotout et al. 2020). This paper deals with metabasites from two major tectonostratigraphic units of the Variscan Schwarzwald: the Central and the Southern Schwarzwald Gneiss complexes (CSGC, SSGC) (Kalt et al. 2000). While the amphibolite-facies gneisses of both complexes are derived from Ordovician to Devonian clastic sediments and granitoids (Hanel et al. 1999; Hegner et al. 2001; Kober et al. 2004), the age and origin of their small metabasic inclusions are still not exactly known, since up to now only very limited modern chemical and isotopic data are available (e.g. Klein and Wimmenauer 1984; Büsch et al. 1985; Kalt et al. 1994b; Hegner et al. 2001). Many of these metabasic bodies underwent an eclogite-facies metamorphism before they became metamorphosed under amphibolite-facies conditions at ~ 333 Ma (Suter 1924; Erdmannsdörffer 1938; Eigenfeld-Mende 1948; Klein and Wimmenauer 1984; Kalt et al. 1994b). Furthermore, the CSGC contains an area (located about 10 km to the East of Lahr, near to Hohengeroldseck Castle; Fig. 1) with metabasites that suffered a high-*P*/ultrahigh-*T* (H*P*-UH*T*) granulite-facies metamorphism prior to a L*P*-H*T* amphibolite-facies overprint (Hanel et al. 1993). In this study, we present geochemical data on a large number of metabasic bodies and we will try to interpret the bulk-rock chemical compositions of these bodies with respect to their primary igneous precursor rocks. Furthermore, we will discuss the geodynamic importance of these two types of metabasic rocks within the framework of the Central European Variscan orogen.

Geological setting

Located in the central part of the Variscan collisional belt of Europe (Fig. 1), the crystalline basement of the Schwarzwald consists of four main tectonometamorphic complexes. From north to south, these are the Baden-Baden Zone (BBZ), the CSGC, the Badenweiler-Lenzkirch Zone (BLZ), and the SSGC. All these complexes are older than granitoids with intrusion ages of 330–333 Ma (Altherr et al. 1999, 2000, 2019; Schaltegger 2000).

The BBZ (Fig. 1) consists of three tectonic slices with different low-*P* and medium-*P* metamorphic overprints (Wickert et al. 1990). The CSGC comprises the following lithologies: (1) Migmatic paragneisses poor in K-feldspar (e.g. Mehnert and Büsch 1982); (2) orthogneisses of tonalitic to granodioritic compositions (Todt and Büsch 1981); (3) minor metabasite lenses that often show relic eclogitic parageneses (Erdmannsdörffer 1938; Eigenfeld-Mende 1948; Hanus et al. 1984; Klein and Wimmenauer 1984; Kalt et al. 1994b; Chen et al. 2003); (4) garnet-spinel peridotites and garnet pyroxenites (Kalt et al. 1995; Kalt and Altherr 1996); (5) retrograde H*P*-UH*T* granulites (Flöttmann and Kleinschmidt 1989; Büsch and Mehnert 1991; Hanel et al. 1993; Marschall et al. 2003); (6) leucocratic gneisses that are frequently associated with amphibolites (without eclogitic relics) and calcsilicate rocks (Wimmenauer 1988; Wimmenauer and Lim 1988). Most, if not all of the protoliths of these metamorphic rocks are of Early Paleozoic age (e.g. Todt and Büsch 1981; Kalt et al. 1994a; Hanel et al. 1999; Chen et al. 2000; Kober et al. 2004).

Eclogitic parageneses in mafic rocks of the CSGC were formed at minimum pressures of 1.6 GPa and peak temperatures of 670–750 °C (Kalt et al. 1994b). A minimum age of this H*P*-H*T* event was given by three Sm–Nd (Cpx-)Grt-WR isochrons of 332 ± 13, 334 ± 11 and 337 ± 6 Ma (Kalt et al. 1994b). Moreover, Chen et al. (2003) gave two Sm–Nd Grt1-Grt2-WR isochrons of 340 ± 8 and 348 ± 3 Ma (Grt1 and Grt2 are mildly and strongly leached garnet fractions, respectively; WR = whole rock). Such Sm–Nd age values may, however, well be the result of retrograde Sm–Nd diffusion in garnet as was shown for eclogites from the Bixiling massif in China (An et al. 2018).

In marked contrast with the eclogites, H*P*-UH*T* granulites were formed at pressures of 1.4–1.8 GPa and temperatures of 950–1010 °C (Büsch and Mehnert 1991; Marschall et al. 2003). Hanel et al. (1993) reported a $^{207}Pb^*/^{206}Pb^*$ evaporation age of 341 ± 19 Ma on zircons from small retrograde mafic granulite bodies located to the East of Lahr (Fig. 1).

The assembled tectonic units of the CSGC experienced a common L*P*-H*T* metamorphism and anatexis at 0.4–0.5 GPa and 675–690 °C (Mehnert and Büsch 1982). The age of this metamorphism is between 330 and 333 Ma as indicated by concordant U–Pb ages on monazite and by Rb–Sr thin slab dating of migmatites (Kalt et al. 1994a). Note, however, that Weyer et al. (1999) reported a higher U–Pb age of 341 ± 2 Ma for monazite from a kinzigitic gneiss rich in garnet and pinitized cordierite.

The BLZ (Fig. 1) is a complex tectonic zone with right-lateral transpressive movement to the SE. It consists of several tectonic units that were either metamorphosed at low pressure and medium to very low temperature or are virtually non-metamorphic. The BLZ is cut by intrusions of deformed and undeformed granites with U–Pb ages on zircon between 331 and 333 Ma (Schaltegger 2000; Altherr et al. 2019).

The SSGC consists of four units of amphibolite-facies rocks (Fig. 1): (1) Wehra-Wiesetal unit comprising migmatic gneisses, amphibolites, metagabbros and meta-anorthosites (Wimmenauer 1984; Sebert and Wimmenauer 1992); (2) Todtmoos unit consisting of gneisses, leptynites, amphibolites and small bodies of spinel peridotites (Hegner et al. 2001; Marschall et al. 2003); (3) Murgtal unit with anatectic gneisses, pyroxene gneisses, quartzites and calc-silicate rocks (Wimmenauer 1984); (4) Monotonous unit with plagioclase-biotite gneisses that are mostly devoid of K-feldspar and may be cordierite-bearing (Wimmenauer 1984). This unit also comprises amphibolitic metabasites that may contain eclogite relics (Suter 1924).

Sampling strategy and analytical techniques

During or after metamorphism, the chemical composition of an igneous rock may change, in particular by the influence of aqueous fluids or melts, but also by solid-state diffusion. Primarily, such metasomatic changes are to be expected near the contacts of rock bodies that are chemically very different. In the given case of small metabasic rock bodies (< 800 m in diameter) that are enclosed within biotite-quartz-feldspar-rich gneisses, this problem becomes highly significant. To reduce possible negative consequences, we only sampled metabasic bodies measuring at least ~ 10 m in diameter, and we tried to get samples from the inner parts of these bodies at some distance from their contacts to gneisses. However, it was almost inevitable to avoid samples showing petrographic indications of a late-stage hydrothermal overprint, such as sericitization of plagioclase or chloritization of amphibole, orthopyroxene, biotite or garnet. Moreover, we tried to avoid samples from metabasic rock bodies that are located near to late- and post-Variscan hydrothermal veins with Pb–Zn-Cu or Co–Ni-Ag-Bi-U mineralizations (e.g. Bons et al. 2014; Epp et al. 2019). Nevertheless, while 45 of our samples have Pb concentrations of 2.4–18.2 µg/g, we found three samples that contain unusually high concentrations of 58–190 µg/g Pb possibly indicating the influence of late hydrothermal fluids. Chemical compositions and coordinates (WGS84) of the analysed samples are given in Table S1.

For bulk-rock analysis, specimens were processed in a steel jaw crusher. After splitting, about 50 g aliquots were ground in an agate mill. The powders were dried at 105 °C for about 24 h. Major elements analyses were determined by wavelength dispersive X-ray fluorescence (WDXRF) spectrometry on lithiumtetraborate fusion disks (1.5 g rock powder + 7.5 g *di*-Lithiumtetraborate). International rock standards were used for calibration.

Trace element concentrations on 22 samples were determined by inductively coupled plasma mass spectrometry (ICP-MS) using a VG PlasmaQuad PQ1 equipped with a VG multi-channel-analyzer at the Institute of Geosciences, Kiel University, Germany. For a description of the instrument configuration and operating conditions see Garbe-Schönberg (1993). Another 26 samples were analyzed by LA-ICP-MS at the Geozentrum Nordbayern (GZN), the University of Erlangen-Nürnberg, with a single-collector quadrupole Agilent 7500c inductively coupled plasma mass spectrometry system equipped with an Analyte Excite 193 nm laser ablation system. Measurements were performed on lithium borate fusion disks using a spot diameter of 85 µm and a laser frequency of 20 Hz. Bulk-rock SiO_2 concentrations from XRF were used as internal standards. For external calibration, the glass reference material NIST SRM 612 with the values of Pearce et al. (1997) was used. Further details are given in Brätz and Klemd (2002).

Mineral analyses were carried out at the Institute of Earth Sciences at Heidelberg using a CAMECA SX51 electron microprobe equipped with five wavelength-dispersive spectrometers. Operating conditions were 15 kV accelerating voltage, 20 nA beam current and a beam diameter of ~ 1 µm. Counting times were 10 s for Si, Al, Fe, Mn, Ca, Na, and K, but 20 s for Mg, Ti, and Cr. Matrix corrections were done online with the PAP algorithm (Pouchou and Pichoir 1984, 1985).

Back-scattered electron images were obtained using a LEO 440 scanning electron microscope with an attached Oxford Inca energy-dispersive analytical system at Heidelberg.

Results

Petrography and metamorphic reactions

In the petrographic description of the investigated metabasites, mineral abbreviations as given in Whitney and Evans (2010) and Roman numerals and letters are used to describe different mineral generations and textural locations, respectively. Based on their petrographic characteristics, the metabasites can formally be classified into three groups. Group 1 metabasites show textural and/or mineralogical relics of a former H*P*-H*T* eclogite-facies stage overprinted to variable degrees by a later L*P*-H*T* amphibolite-facies metamorphism. Group 2 comprises equilibrated amphibolites without any eclogitic relics. These rocks either did not undergo a high

P/*T* stage or were completely recrystallized during the L*P*-H*T* event. Group 3 metabasites are former H*P*-UH*T* granulites that were also overprinted by a L*P*-H*T* amphibolite-facies metamorphism.

In group 1 metabasites, four sequential metamorphic stages can be recognized: (I) An eclogite stage at *P*–*T* conditions of > 1.6 GPa and 670–750 °C (Kalt et al. 1994b), (II) retrograde reactions in partial volumes of the rocks, caused by pressure release during near-isothermal conditions, (III) an amphibolite-facies stage at 0.4–0.5 GPa and 675–690 °C (Mehnert and Büsch 1982; Kalt et al. 1994a), and (IV) a multistage retrograde hydrothermal evolution at greenschist- to zeolite-facies conditions (Klein and Wimmenauer 1984; Kalt et al. 1994b). The eclogite stage I is documented by relics of high-*P*/*T* minerals, such as garnet (Grt I), omphacite (Cpx I) and rutile (Rt I) that are eventually accompanied by kyanite (Ky I), quartz (Qtz I), pargasitic amphibole (Amp I), epidote (Ep I), and rare phengite (Phe I). Garnet I grains may contain inclusions of Cpx I, Rt I, Amp I, Ep I, Zrn I, Ap I, and Qtz I. Omphacite grains (X_{Jad} = 0.32–0.47) are rarely preserved and may contain inclusions of Rt I and Grt I. Rutile I may be partially altered to ilmenite and/or titanite (Erdmannsdörffer 1938; Eigenfeld-Mende 1948; Klein and Wimmenauer 1984; Kalt et al. 1994b). Light-optical pictures of some of the most preserved eclogites are given in Fig. 2a–d.

During exhumation of the eclogites, a decrease in *P* and a variable increase in the amount of infiltrating H_2O-rich fluids caused a number of metasomatic retrograde alterations (Klein and Wimmenauer 1984; Kalt et al. 1994b):

1.Omphacite (Cpx Ia1) is often partly or even completely replaced by diopsidic pyroxene (Cpx IIa) and oligoclase (Pl IIa). In samples, that still contain *original* omphacite (Cpx Ia) the beginning of this transformation is often documented by domains in which a secondary, less Na-rich omphacite (Cpx Ia2) contains tiny elongated crystals (< 10 µm) of nearly pure albite (Pl Ia) (Fig. 2e–h). In most cases, however, omphacitic Cpx Ia was completely transformed to a diablastic intergrowth of Cpx IIa and Pl IIa. Such transformations need the local addition of SiO_2 that was most probably introduced by an H_2O-rich fluid phase:

$$\text{Cpx Ia (Omp)} + \text{SiO}_2\text{(aq)} = \text{Cpx Ib/IIa} + \text{Pl Ib/IIa}. \quad (1)$$

2. Decomposition of garnet I started with two reactions. At places where Qtz I was in contact with Grt I, a two-layer corona was formed. Garnet relics are surrounded by intermediate plagioclase (Pl IIb), followed by an outer layer of orthopyroxene (Opx IIb) and intermediate plagioclase (Pl IIb), eventually accompanied by clinopyroxene (Cpx IIb) and amphibole (Amp IIb) (Fig. 3a–d). This suggests the reaction:

$$\text{Grt I} + \text{Qtz I} + \text{Na}_2\text{O} \pm \text{H}_2\text{O} \pm \text{K}_2\text{O} = \text{Pl IIb} + \text{Opx IIb} \pm \text{Cpx IIb} \pm \text{Amp IIb}. \quad (2)$$

Na_2O was probably derived from decomposing omphacite, but could as well be introduced by an H_2O-rich fluid phase.

The second garnet-consuming reaction took place at contacts of Grt I and Cpx Ia/Ib, where a kelyphite or symplectite consisting of amphibole, oligoclase/andesine and minor spinel, sometimes accompanied by ilmenite was formed (Fig. 3e–f):

$$\text{Grt I} + \text{Na} - \text{rich Cpx I} + \text{K}_2\text{O} + \text{H}_2\text{O} = \text{Amp IIc} + \text{Pl IIc} \pm \text{Spl IIc} \pm \text{Ilm IIc} \quad (3)$$

3. In more Al-rich retrograde eclogites, Ky I grains are present and may be partially mantled or entirely replaced by symplectites (S IId) of An-rich plagioclase (Pl IId) and spinel (Spl IId) which are encircled by an outer zone of Pl IId (Fig. 4a–c). These symplectites may contain smaller volumes, where corundum (Crn IId) or sapphirine (Spr IId) occur instead of spinel. While Crn IId occurs rarely along the contacts to relict Ky I, Spr IId was found in some samples near to the outer rim of the symplectites (Fig. 4d–g). Thus, these three Al-rich phases reflect a variation in the local chemical potentials of SiO_2, Al_2O_3, CaO, Na_2O, MgO and FeO, producing the reaction

$$\text{Ky I} + (\text{Mg, Fe})\text{O} + \text{CaO} + \text{Na}_2\text{O} \pm \text{SiO}_2 \pm \text{Al}_2\text{O}_3 = \text{Pl IId} + \text{Spl IId} \pm \text{Crn IId} \pm \text{Spr IId} \quad (4)$$

The symplectite volume is always surrounded by an outer corona of Pl IId (Fig. 4c) that shows a strong outward decrease in An content. At places near to Ilm IId, the Ky-replacing symplectites may also contain minor amounts of relatively Mg-rich staurolite (St IId) (Fig. 4h).

4. In the more intensely retrograded eclogites, symplectites of amphibole + plagioclase ± ilmenite are formed, most probably by the reaction

$$\text{Grt I} + \text{Cpx Ib} + \text{Rt I} + \text{H}_2\text{O} + \text{K}_2\text{O} = \text{Amp IIe} + \text{Pl IIe} \pm \text{Ilm IIe}. \quad (5)$$

These symplectites may show increasing recrystallization to coarser aggregates of Amp III + Pl III ± Ilm III.

5.At a later stage, ilmenite may be replaced by titanite and magnetite according to the following oxidation and hydration reactions:

$$\text{Amp IIe/III} + \text{Ilm IIc/IIe/III} + \text{O}_2 = \text{Tit III} + \text{Mgt III} + \text{Qz III} + \text{H}_2\text{O} \quad (6a)$$

and

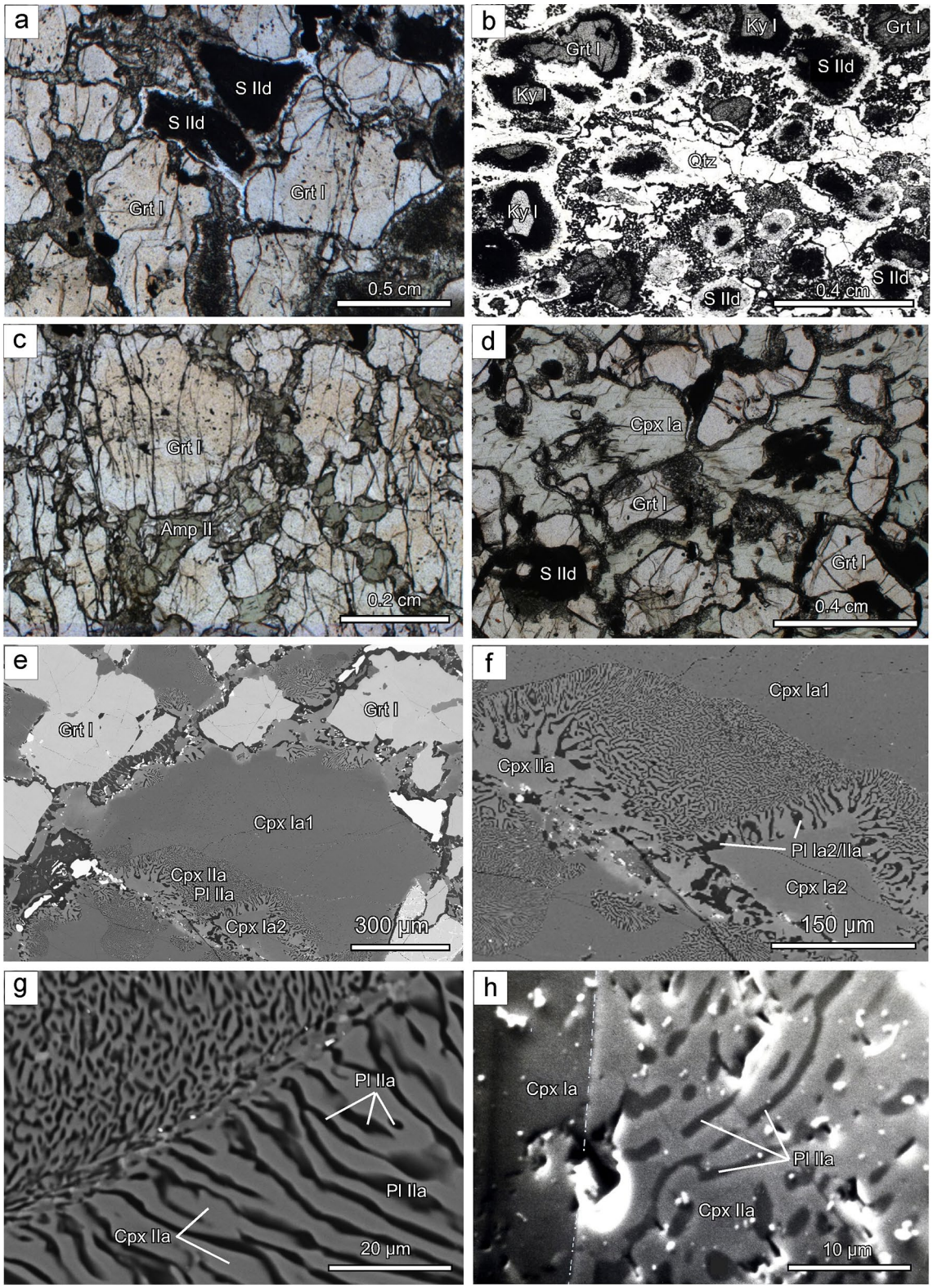

Fig. 2 **a** Garnet I and symplectite after Ky I (S IId) consisting of Spl IId, Pl IId and minor amounts of Spr IId (sample OW1). **b** Garnet I and relict Ky I surrounded by a symplectite of Spl IId + Pl IId ± Spr IId (sample OW2). **c** Garnet I and Amp II (sample 25e-1). d Grt I and Cpx Ia together with symplectite S IId (sample HA602). **e** Large grain of Cpx Ia with partial alterations to Cpx Ib/IIa and Pl IIa along the outer border (sample LO1). **f** Enlargement of Fig. 2e. **g** Symplectite of Cpx IIa and Pl IIa produced by allochemical alteration of Cpx Ia (sample LO1). See text for further explanation. **h** Border between relict Cpx Ia and symplectite between Cpx IIa and Pl IIa (sample TN11)

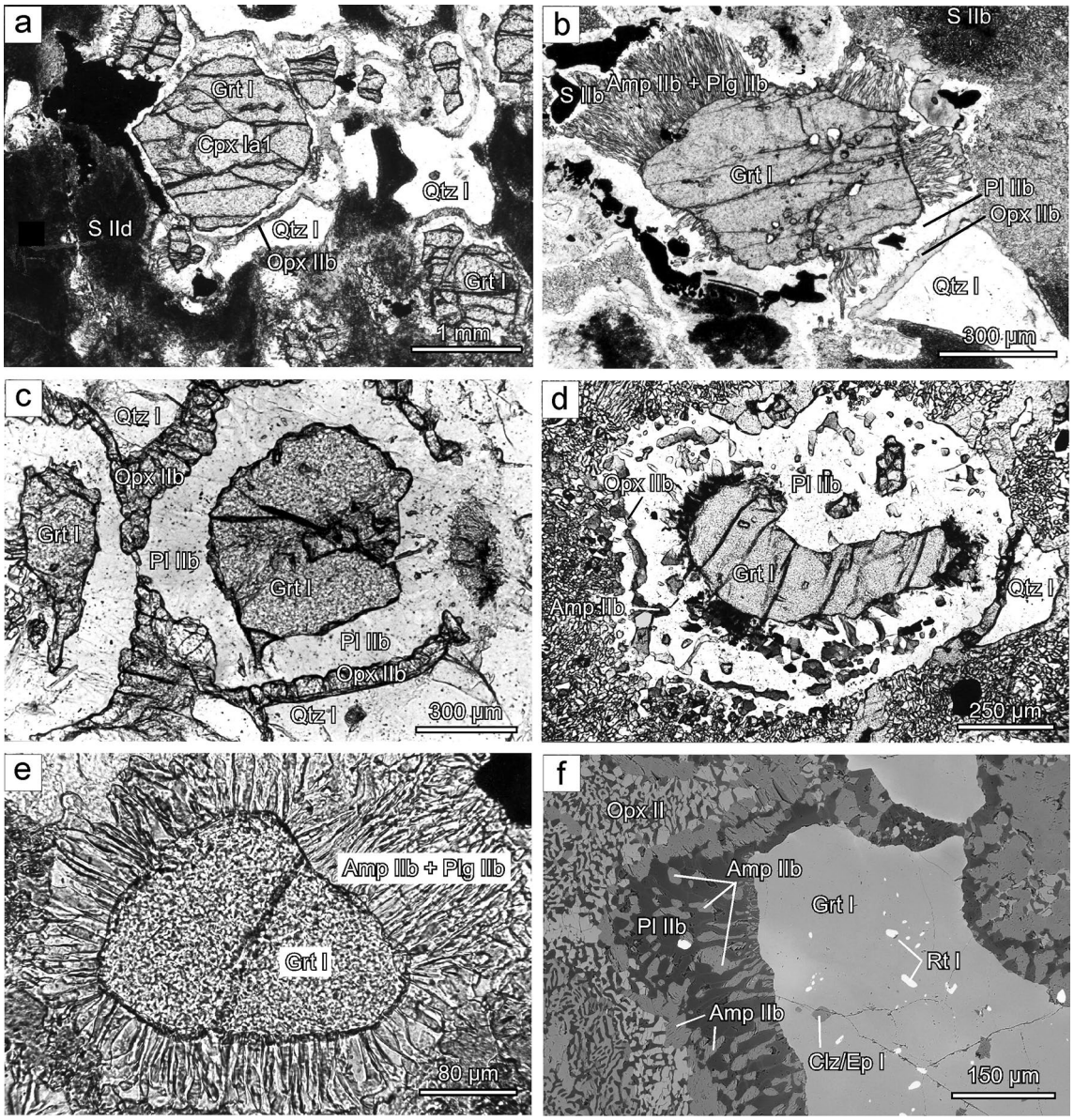

Fig. 3 **a** Garnet I with an inclusion of omphacite (Cpx Ia1) beside symplectite after Ky I (S IId) (sample FE22). **b** Garnet I with a broad corona of Amp IIb and Plg IIb at the boundary to former Ky I (now S IIb), but a relatively thin corona towards Qtz I (sample FSE9). **c** Grt I surrounded by a two-layer corona of Pl IIb + Opx IIb ± Cpx IIb (sample HA19). **d** Garnet I with a secondary envelope of Pl IIb, Opx IIb and Amp IIb generated by reaction between Grt I and Qtz I (sample O3). **e** Relict Grt I with a corona of Pl IIb + Amp IIb (sample H10). **f** Garnet I with inclusions of Rt I and Clz/Ep I surrounded by a corona of Amp IIb and Pl IIb. On the left-hand side, an intergrowth of Opx IIb and Plg IIb is present (sample HA84)

$$\text{Cpx II} + \text{Ilm IIc} + \text{Qz I} + \text{H}_2\text{O} = \text{Amp III} + \text{Tit III}. \quad (6b)$$

At places, rutile was also directly transformed to titanite, or it is surrounded by ilmenite that itself may be overgrown by titanite. It is obvious that these transformations of rutile were dependent on variable fO_2 and fH_2O.

6.Biotite III was locally formed around Grt I and indicates the introduction of larger amounts of K_2O. In more intensively overprinted eclogites, Bio III may form aggregates with Amp III and Pl III.

All the retrograde reaction textures observed in overprinted eclogites of the Schwarzwald are also known from retrogressed H*P*-H*T* eclogites at many other worldwide

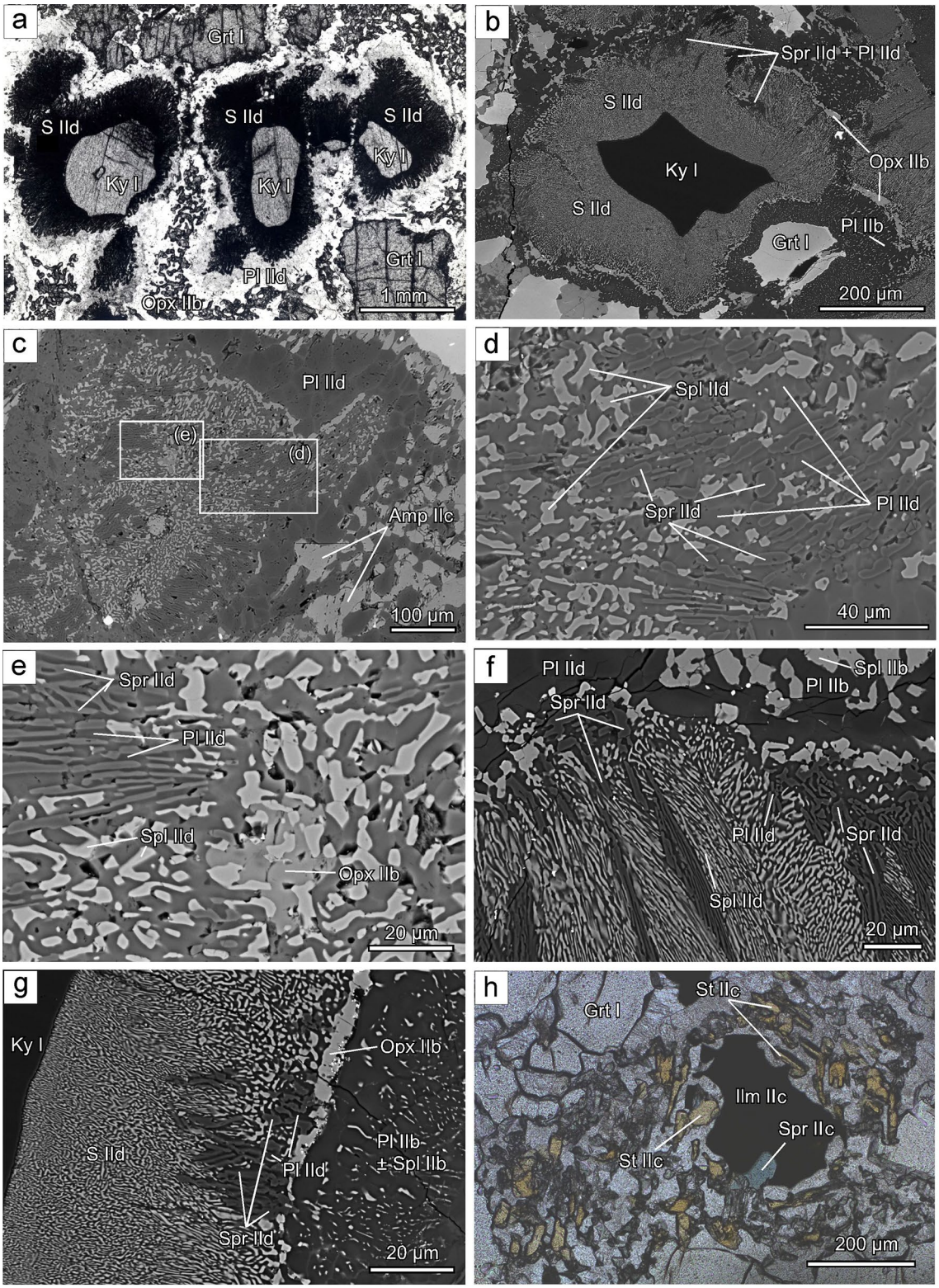

localities (e.g. Enami et al. 1993; Godard and Mabit 1998; Nakamura 2002; Săbău et al. 2002; Anderson and Moecher 2007; Faryad et al. 2013; Hyppolito et al. 2018).

Group 2 metabasites are amphibolites without any mineralogical or textural relics of an earlier eclogitic stage. Either these rocks were never eclogites or they recrystallized completely during the amphibolite-facies event. Textures are

◂**Fig. 4** **a** Relics of Ky I enclosed by symplectites of Spl IId + Pl IId. The inner parts of these symplectites (S IId) may contain additional Crn IId, while the outer parts often contain additional Spr IId. The symplectites are surrounded by a zone of Pl IId (sample OW2, Wassereck, about 5 km N of Oberwolfach). **b** Relic kyanite I surrounded by a symplectite (S IId) of Spl IId + Pl IId ± Spr IId. Note that Spr IId only occurs locally in the outer parts of this symplectite. Garnet is surrounded by Pl IIb ± Spl IIb + Opx IIb (sample HA602). **c** Pseudomorph of Spl IId + Pl IId ± Spr IId after Ky I surrounded by Pl IId. Fields (d) and (e) give positions of Figs. 4d and 4e (sample OW1). **d** and **e** Symplectites of Pl IId and either Spl IId or Spr IId (sample OW1). **f** Symplectite of Pl IId and Spl IId or Spr IId (sample HA602). **g** Traverse from Ky I, surrounded by symplectite S IId (Spl IId + Pl IId), locally followed by Spr IId + Pl IId into a zone of Opx IIb + Pl IIb ± Spl IIb generated by decomposition of Grt I (sample HA602). **h** St IId, Spr IId and Ilm IId as reaction products from Ky I (sample 25e-1, Schirleberg, ENE of Wolfach)

foliated to massive. Besides Amp III and Pl III, these rocks may contain diopsidic pyroxene (Cpx III), Bio III, Qtz III, Tit III, Ilm III, Ap III and Zrn III. Amphibole III shows dark greenish to brownish colours and Pl III is polysynthetically twinned. Both phases contain abundant inclusions of all the other phases.

Granulite-facies assemblages in metabasic rocks of group 3 are relatively coarse grained and show a former paragenesis of Grt I + Cpx I + Pl I + Ky I ± Qz I ± Rt I ± Ilm I ± Ap I ± Zrn I (Hanel et al. 1993). At a later stage, during decompression, but still without H_2O, the following reaction took place:

$$\text{Grt I} + \text{Qtz I} = \text{Opx IIa} + \text{Pl IIa} \pm \text{Cpx IIa} \quad (7a)$$

Later hydration promoted the formation of symplectite rims around Grt I according to the allochemical reaction

$$\text{Grt I} + \text{Cpx I} + H_2O + K_2O = \text{Opx IIb} + \text{Pl IIb} + \text{Amp IIb} \pm \text{Cpx IIb}. \quad (7b)$$

Furthermore, kyanite was allochemically transformed to An-rich plagioclase and spinel:

$$\text{Ky I} + (\text{Mg, Fe})O + CaO + Na_2O \pm SiO_2 \pm Al_2O_3 = \text{Pl IIc} + \text{Spl IIc} \quad (7c)$$

Metabasites of all three groups may show an allochemical hydrothermal overprint. It is well known that in the Schwarzwald such low-temperature overprints of Variscan crystalline rocks and of Upper Carboniferous sediments took place in Late Carbonifereous, Permo-Triassic as well as in Late Jurassic to Cretaceous times (e.g. Lippolt and Kirsch 1994; Glodny and Grauert 2009; Brockamp et al. 2015). In particular, An-rich plagioclase is partially or completely replaced by sericite IV. Moreover, amphibole, orthopyroxene, biotite and garnet may be partially chlorititized (Chl IV). Rarely, veins of prehnite (Prh IV) have been observed in strongly amphibolitized samples.

Mineral chemistry of retrograde eclogites and amphibolites

Garnet I grains show variable compositions ($Alm_{23–53}Prp_{16–40}Grs_{15–36}Sps_{0.4–2.0}Adr_{1–8}$), depending on bulk-rock chemistry and retrograde evolution (Table 1). Core-to-rim zoning patterns are characterized by nearly constant compositions of broad cores and narrow (< 100 µm) rims with increasing Prp and Alm, but decreasing Grs components, while Sps and Adr components are nearly constant or may vary unsystematically.

Clinopyroxene I is an omphacite (Table 1), whereby the highest NaO contents (4.0–6.9 wt %) are found in the cores of larger grains (Cpx Ia1) and in smaller Cpx Ia1 inclusions in garnet. Cpx Ia2 may contain small albite grains and may form rims around Cpx Ia1 or small grains in the matrix. It is characterized by significantly lower NaO contents (1.2–4.0 wt %). Diablastic Cpx IIa is diopside showing low Na_2O contents (0.1–1.2 wt %). If present, Cpx III is diopside with very low Na_2O contents (0.3–0.5 wt %). Rutile I is generally characterized by significant concentrations of Fe_2O_3 (0.4–1.1 wt %).

Orthopyroxene IIb that was formed by an allochemical reaction between Grt I and Qtz I has an approximate composition of $Mg_{0.93}Fe^{2+}_{0.99}Mn_{0.03}Ca0_{.03}Na_{0.01}{}^{VI}Al_{0.01}{}^{IV}Al_{0.02}Si_{1.98}O_6$, whereby the ratio of $Mg/(Mg + Fe^{2+})$ may vary from sample to sample or from position to position within a thin section (Table 1).

Plagioclase compositions are variable, depending on the textural position. While Pl Ib is nearly pure albite, Pl IIa is oligoclase and Pl IIb is labradorite. Plagioclase IIc, formed by the reaction between Grt I and Cpx I, is oligoclase or andesine. Plagioclase IId within the pseudomorphs after kyanite is very rich in anorthite component (An_{80-95}), while Pl IIe and Pl III show intermediate compositions, depending on the amount of coexisting amphibole.

Spinel IIc and IId compositions are approximately intermediate between hercynite and spinel in the narrower sense. Corundum IId located in the inner parts of the plagioclase-bearing symplectites after kyanite I contains an appreciable amount of Fe_2O_3 (0.4–1.0 wt %) but is nearly free of Cr_2O_3 (< 0.1 wt %). Ilmenite IIc and IId contain small amounts of hematite and geikielite, while ilmenite III is characterized by significant contents of the pyrophanite component.

Sapphirine IId is slightly peraluminous with the composition $(Mg_{2.82–3.01}Fe^{2+}_{0.54–0.41}Mn_{0.02–0.01})(Al_{8.97–8.94}Cr_{0.02–0.03}Fe^{3+}_{0.27–0.19})Si_{1.35–1.42}O_{20}$. Staurolite IId is relatively rich in MgO. On the assumption of 44 O and 4 OH (Griffen et al. 1982), we got the formula $(Mg_{1.77}Fe_{2.19}Mn_{0.02}Zn_{0.02})(Cr_{0.03}Al_{17.37})(Si_{6.87}Al_{1.13})O_{44}(OH)_4$.

Table 1 Selected chemical analyses of garnet, clinopyroxene, orthopyroxene, and amphibole in group 1 and group 2 metabasites from the Schwarzwald

Mineral	Grt	Grt	Grt	Grt	Cpx	Cpx	Cpx	Cpx	Opx	Amp	Amp	Amp	Amp	Amp	Amp	Amp
Stage	I	I	I	I	Ia	IIa	IIb	III	IIb	I	IIb	IIc	III	III	III	III
Domain	Core	Rim	Core	Rim	Core	Core	Core	Core	Core	Core	Core	Core	Rim	Rim	Core	Rim
Sample	FE10	FE10	SP56	SP56	FE10	FE10	SP56	GÖ5	SP56	SP56	SP56	SP56	GÖ2	TO51	ZEH7	ZEH7
SiO_2	39.59	39.52	39.02	39.26	55.40	52.80	52.35	51.97	50.66	41.36	42.92	43.57	45.09	44.68	43.52	46.22
TiO_2	0.04	0.02	0.01	0.05	0.15	0.05	0.05	0.02	0.00	1.02	0.27	0.12	0.98	1.29	1.12	0.83
Al_2O_3	22.19	22.15	21.91	21.64	12.15	4.63	1.36	0.90	0.81	13.68	13.65	12.17	10.17	9.70	10.67	8.33
Cr_2O_3	0.00	0.00	0.01	0.00	0.02	0.04	0.02	0.02	0.00	0.16	0.02	0.07	0.11	0.00	0.03	0.02
Fe_2O_3	0.70	1.34	0.86	0.52	0.00	0.18	0.13	0.83	0.00	4.57	5.56	6.09	5.53	6.02	5.34	4.89
FeO	20.43	20.26	19.10	20.82	5.36	5.16	11.39	11.08	30.21	9.63	11.67	12.79	11.62	12.65	11.21	10.26
MnO	0.30	0.24	0.31	0.72	0.09	0.13	0.36	0.52	0.89	0.22	0.36	0.30	0.34	0.46	0.21	0.26
MgO	9.20	10.58	7.08	6.35	7.19	13.37	11.93	11.20	15.99	11.71	10.79	10.14	11.62	9.77	11.49	13.38
CaO	8.00	6.19	11.42	11.02	12.61	22.52	22.26	22.77	0.59	11.44	10.32	10.36	10.55	11.01	11.90	11.68
Na_2O	0.00	0.00	0.00	0.00	6.87	1.12	0.23	0.31	0.03	3.44	2.22	1.79	1.32	1.10	1.34	1.16
K_2O	0.00	0.00	0.00	0.00	0.00	0.00	0.00	0.00	0.00	0.51	0.34	0.45	0.31	0.52	0.68	0.37
H_2O*	0.00	0.00	0.00	0.00	0.00	0.00	0.00	0.00	0.00	2.03	2.04	2.02	2.04	2.01	2.02	2.04
Total	100.45	100.30	99.72	100.38	99.84	100.00	100.08	99.62	99.18	99.77	100.15	99.88	99.66	99.21	99.52	99.45
Si	2.991	2.977	2.986	3.005	1.979	1.936	1.975	1.977	1.983	6.121	6.318	6.466	6.644	6.674	6.466	6.788
Ti	0.002	0.001	0.001	0.003	0.004	0.001	0.001	0.001	0.000	0.114	0.030	0.013	0.108	0.145	0.125	0.091
Al	1.975	1.967	1.976	1.953	0.511	0.200	0.060	0.040	0.037	2.386	2.368	2.129	1.766	1.708	1.868	1.442
Cr	0.000	0.000	0.001	0.000	0.001	0.001	0.001	0.001	0.000	0.019	0.002	0.008	0.013	0.000	0.004	0.002
Fe^{3+}	0.040	0.076	0.050	0.030	0.000	0.005	0.004	0.024	0.000	0.510	0.616	0.680	6.613	0.677	0.597	0.540
Fe^{2+}	1.290	1.276	1.222	1.333	0.160	0.158	0.360	0.352	0.989	1.191	1.436	1.587	1.431	1.580	1.392	1.260
Mn	0.019	0.015	0.020	0.047	0.003	0.004	0.012	0.017	0.030	0.028	0.045	0.038	0.042	0.058	0.027	0.033
Mg	1.036	1.188	0.808	0.725	0.383	0.731	0.670	0.636	0.933	2.584	2.368	2.243	2.552	2.176	2.546	2.932
Ca	0.647	0.500	0.936	0.904	0.483	0.884	0.900	0.929	0.025	1.814	1.628	1.647	1.665	1.762	1.894	1.837
Na	0.000	0.000	0.000	0.000	0.476	0.080	0.017	0.023	0.002	0.987	0.634	0.515	0.376	0.319	0.387	0.331
K	0.000	0.000	0.000	0.000	0.000	0.000	0.000	0.000	0.000	0.096	0.064	0.085	0.058	0.099	0.128	0.070
Total	8.000	8.000	8.000	8.000	4.000	4.000	4.000	4.000	3.999	15.850	15.509	15.411	15.268	15.198	15.434	15.326

Formulae were calculated on the basis of 12 oxygens and 8 cations for garnet, 6 oxygens and 4 cations for pyroxenes, and 22 oxygen and 2 OH^- for amphibole. A ratio of $Fe^{3+}/(Fe^{2+}+Fe^{3+})=0.3$ was assumed for amphibole analyses. H_2O* is calculated H_2O content

Amphibole analyses are given in Table 1. While rare Amp I is a ferroan pargasite, the compositions of Amp IIb, IIc, and IIe are very similar and are characterized by relatively high contents of Al_2O_3 (~ 12–15 wt %) combined with low contents in TiO_2 (< 0.35 wt %). In marked contrast, Amp III compositions show lower Al_2O_3 (8–10 wt %), but higher TiO_2 concentrations (0.7–1.8 wt %). While concentrations of Cl are always < 0.10 wt %, those of F may reach 0.35 wt %, but in most samples are also below 0.10 wt%.

Epidote/clinozoisite I is relatively rare and mostly occurs as inclusion in Grt I, where it is relatively rich in the pistacite component (e.g. Fe^{3+} = 0.29 cpfu).

Titanite III is characterized by significant contents of Al_2O_3 (0.64–1.39 wt%), Fe_2O_3 (0.38–1.21) and F (0.10–0.41 wt%), suggesting the presence of three components: Titanite s.str. [$CaTiSiO_4O$], (Al,Fe^{3+})-OH titanite [Ca(Al,Fe^{3+})SiO_4OH], and (Al,Fe^{3+})-F titanite [Ca(Al,Fe^{3+})SiO_4F].

Biotite III compositions calculated on the basis of 10 oxygen, 2 OH^-, and $Fe^{2+}/(Fe^{2+}+Fe^{3+})=0.8$ are characterized by TiO_2 contents of 3.3–4.9 wt % and mg# values [= Mg/(Mg + Fe^{2+})] of 0.53–0.61. Na_2O and K_2O concentrations are 0.13–0.27 wt % and 8.2–9.1 wt%, respectively, suggesting only minor alteration.

Chlorite IV grains show variable compositions, depending on their textural position. Within a sample, the mg# values are highest for chlorites formed from Opx IIb, intermediate for those formed from Amp II/III, and lowest for those formed from Bio III.

Mineral chemistry of former H*P*-UH*T* granulites

Garnet I relics show minor zoning with mg# values falling from core to rim, while Ca stays nearly constant (Table 2). Cpx I grains show nearly constant compositions with jadeite contents of about 22 mol %. At places, however, Al_2O_3 and/or Na_2O contents are variably lower, most probably due to recrystallization at lower *P*–*T* conditions. Cpx IIa and IIb grains are diopside (Table 2). Opx IIa and IIb are characterized by moderate contents of CaO (0.4–0.6 wt %).

Plagioclase compositions (Table 2) are variable depending on the textural position. Plagioclase I, IIa, and IIb have andesine to labradorite compositions, while Pl IIc formed together with spinel IIc from kyanite I has $An_{80–90}$. Amphibole IIb is pargasitic with F and Cl contents generally below 0.10 wt % (Table 2).

Bulk-rock chemistry of metabasites

Bulk-rock analyses for selected samples are given in Table 3 and analyses of all samples and of their coordinates are given in Table S1. In a TAS diagram (Le Maitre 2002), the samples are located in or near to the fields of basalt and basaltic andesite (Fig. 5a). Some samples, however, are characterized by very low SiO_2 values of 43–47 wt % and plot into the field of picrobasalts. Values of Mg# [Mg# = 100 × molar (MgO/(MgO + FeO_{tot}))] of samples from group 1 and 2 show a continuous range from 69.8 to 38.4 and many of these samples are therefore considerably fractionated. The sub-alkaline character of most of the samples also becomes apparent in the nomenclature diagram of SiO_2 vs Nb/Y (Winchester and Floyd 1977) (Fig. 5b). In the diagram of P_2O_5 vs Zr after Winchester and Floyd (1976) (Fig. 5c), most of the samples are located in the field for subalkaline basalts. In the

Table 2 Selected chemical analyses of garnet, clinopyroxene, orthopyroxene, ilmenite, amphibole and plagioclase in mafic metagranulites

Mineral	Grt	Grt	Cpx	Cpx	Cpx	Cpx	Cpx	Opx	Opx	Ilm	Amp	Amp	Pl	Pl	Pl
Stage	I	I	I	I/II	I/II	IIa	IIb	IIa	IIb	I	IIb	IIb	IIa	IIb	IIc
Sample	LA41	LA41	LA41	LA41	LA41	LA41	LA41	LA41	LA41	LA41	LA41	LA41	LA41	LA41	LA41
SiO_2	39.86	39.31	51.66	50.34	50.18	51.31	52.66	53.22	53.98	0.00	42.34	41.77	57.98	56.84	45.57
TiO_2	0.08	0.06	0.47	0.33	0.34	0.46	0.20	0.00	0.03	53.53	1.03	0.97	n.a	n.a	n.a
Al_2O_3	22.38	22.02	9.76	9.41	9.29	4.44	2.75	1.77	2.97	0.00	14.84	15.54	26.95	27.38	34.85
Cr_2O_3	0.06	0.13	0.09	0.10	0.01	0.04	0.10	0.00	0.08	0.08	0.06	0.10	n.a	n.a	n.a
Fe_2O_3	0.87	1.15	0.30	0.53	0.65	0.72	0.05	1.16	0.25	0.00	3.15	3.20	0.24	0.24	0.28
FeO	16.52	17.76	4.28	5.48	5.88	5.86	6.29	16.30	14.15	43.10	6.62	6.71	0.00	0.00	0.00
MnO	0.45	0.59	0.02	0.10	0.13	0.08	0.09	0.31	0.41	0.51	0.09	0.07	n.a	n.a	n.a
MgO	9.80	8.51	10.72	11.72	12.04	13.63	14.49	26.03	27.66	2.27	13.81	13.73	n.a	n.a	n.a
CaO	10.36	10.58	18.98	19.77	19.53	22.07	22.48	0.53	0.44	0.00	11.37	11.45	7.97	8.42	18.16
Na_2O	0.00	0.00	3.13	1.88	1.71	0.71	0.45	0.00	0.03	0.00	2.73	3.02	7.01	6.91	0.93
K_2O	0.00	0.00	0.00	0.00	0.00	0.00	0.00	0.00	0.00	0.00	1.27	0.67	0.16	0.15	0.03
H_2O*	0.00	0.00	0.00	0.00	0.00	0.00	0.00	0.00	0.00	0.00	2.06	2.06	0.00	0.00	0.00
Total	100.38	100.11	99.41	99.66	99.75	99.32	99.57	99.32	100.00	99.49	99.36	99.29	100.31	99.94	99.82
Si	2.983	2.977	1.882	1.845	1.840	.905	1.949	1.945	1.933	0.000	6.166	6.082	2.587	2.552	2.102
Ti	0.005	0.003	0.013	0.009	0.009	0.013	0.006	0.000	0.001	1.002	0.113	0.106	n.c	n.c	n.c
Al	1.974	1.965	0.419	0.407	0.402	0.194	0.120	0.076	0.126	0.000	2.547	2.667	1.417	1.449	1.894
Cr	0.004	0.008	0.003	0.003	0.000	0.001	0.003	0.000	0.002	0.002	0.002	0.012	n.c	n.c	n.c
Fe^{3+}	0.049	0.065	0.008	0.015	0.018	0.020	0.001	0.032	0.007	0.000	0.345	0.350	0.008	0.008	0.010
Fe^{2+}	1.034	1.125	0.130	0.168	0.180	0.182	0.195	0.498	0.424	0.898	0.806	0.817	0.000	0.000	0.000
Mn	0.029	0.038	0.001	0.003	0.004	0.003	0.003	0.010	0.012	0.011	0.011	0.009	n.c	n.c	n.c
Mg	1.093	0.961	0.582	0.640	0.658	0.754	0.799	1.418	1.476	0.084	2.998	2.979	n.c	n.c	n.c
Ca	0.831	0.858	0.741	0.776	0.767	0.878	0.891	0.021	0.017	0.929	1.775	1.787	0.381	0.405	0.897
Na	0.000	0.000	0.221	0.134	0.122	0.051	0.032	0.000	0.002	0.000	0.770	0.853	0.606	0.602	0.083
K	0.000	0.000	0.000	0.000	0.000	0.000	0.000	0.000	0.000	0.000	0.236	0.124	0.009	0.009	0.002
Total	8.000	8.000	4.000	4.000	4.000	4.000	4.000	4.000	4.000	1.997	15.774	15.785	5.008	5.024	4.988

Formulae were calculated on the basis of 12 oxygens and 8 cations for garnet, 6 oxygens and 4 cations for pyroxenes, 3 oxygens and 2 cations for ilmenite, 22 oxygen and 2 OH^- for amphibole, and total Fe as Fe^{3+} and 8 O for plagioclase. A ratio of $Fe^{3+}/(Fe^{2+} + Fe^{3+}) = 0.3$ was assumed for amphibole analyses. H_2O* is calculated water content. Stages I and II correspond to H*P*-UH*T* granulite-facies and amphibolite-facies metamorphism, respectively. See text for further explanation. n.a. = not analysed, n.c. = not calculated

Table 3 Major (wt%) and trace element (μg/g) compositions of selected metabasites from the Schwarzwald

Rock type*	KyE	KyE	KyE	E	E	E	E	E	E	E	A	A	A	A	G
Area	CSGC	CSGC	CSGC	CSGC	CSGC	CSGC	CSGC	CSGC	CSGC	CSGC	CSGC	CSGC	SSGC	SSGC	CSGC
Sample	EM3	SP11	TN14	OP1	OP7	ZEH1	SP50	SP56	FU7	FE10	WO2	FE12	WEH2	GÖ2	LA41
SiO_2	47.90	43.99	43.15	49.56	48.34	53.66	47.21	43.01	43.16	42.06	53.85	49.18	50.59	52.68	47.50
TiO_2	1.39	2.07	1.02	1.41	0.91	0.72	0.53	1.37	1.30	1.10	0.98	1.26	0.84	0.54	0.69
Al_2O_3	20.64	17.77	22.57	15.86	16.61	16.81	15.12	19.63	18.33	18.03	16.51	20.54	17.32	16.17	19.23
Fe_2O_3	1.06	1.83	2.04	2.92	1.50	1.37	1.55	3.88	1.90	2.10	2.00	2.22	2.30	2.16	1.20
FeO	7.81	13.81	10.14	9.32	6.15	7.94	6.26	9.58	9.81	12.25	5.25	7.15	6.42	7.75	5.51
MnO	0.15	0.22	0.14	0.23	0.12	0.18	0.14	0.19	0.18	0.22	0.16	0.16	0.20	0.17	0.13
MgO	6.61	5.40	6.09	7.91	5.99	5.56	9.92	5.57	7.00	10.54	6.36	6.63	6.32	6.24	8.50
CaO	9.15	11.50	11.72	11.17	11.45	9.01	14.18	10.02	12.38	10.67	7.13	8.98	8.86	8.49	12.30
Na_2O	2.06	1.50	1.51	2.40	2.82	1.66	2.51	1.85	1.66	1.05	3.12	2.36	3.04	3.17	2.38
K_2O	0.55	0.25	0.34	0.18	0.57	0.98	0.55	1.91	0.69	0.18	2.14	0.52	1.39	0.58	0.67
P_2O_5	0.06	0.20	0.12	0.10	0.08	0.09	0.12	0.19	0.28	0.06	0.35	0.15	0.19	0.10	0.05
H_2O	1.52	0.83	1.38	0.97	1.87	1.23	2.08	1.89	2.69	1.72	1.55	1.50	1.61	1.08	1.04
CO_2	0.05	n.a	n.a	0.17	2.45	0.10	0.18	0.05	n.a	n.a	0.07	n.a	0.14	0.09	0.10
Total	98.95	99.37	100.22	99.20	98.86	99.64	100.35	99.04	99.38	99.98	99.47	100.65	99.22	99.22	99.30
Mg#	57.35	38.38	47.55	54.13	58.47	51.93	69.79	43.17	52.00	57.06	61.66	56.37	57.03	53.43	69.69
Sc	n.a	44.7	27.4	n.a	n.a	n.a	38.8	n.a	45.8	27.5	n.a	27.1	46.8	41.5	n.a
V	223	500	654	299	279	282	195	291	539	495	229	234	352	322	153
Cr	54	20	78	341	293	55	403	n.a	111	319	243	140	30	66	391
Co	26	46	41	36	34	31	47	36	37	64	28	25	35	38	32
Ni	8	11	24	44	84	4	52	10	15	58	75	26	26	29	154
Cu	17	56	70	36	35	25	33	35	30	20	20	25	54	44	33
Zn	97	n.a	n.a	107	83	92	77	85	n.a	n.a	88	n.a	86	n.a	46
Ga	20	17	22	18	17	18	12	20	24	20	18	21	17	16	17
Y	30	18	6	40	25	23	18	29	42	12	29	22	20	11	16
Cs	7.0	1.7	12.0	2.0	6.0	5.0	1.1	4.0	3.4	2.3	9.0	6.1	17.9	6.0	6.0
Rb	22.0	7.6	12.3	10.0	19.0	35.0	20.7	56.0	25.7	7.1	84.0	10.3	66.8	27.0	31.0
Ba	120	48	72	48	93	280	134	290	151	44	428	119	251	105	118
Th	0.50	0.80	1.13	0.70	0.30	1.70	1.62	0.70	0.42	3.35	7.60	0.55	1.38	0.30	0.70
U	0.2	0.28	0.47	0.30	0.70	0.70	0.42	0.30	0.10	0.29	2.80	0.33	0.56	0.20	0.20
Nb	5.9	7.3	2.5	2.1	1.3	3.8	2.6	7.2	8.4	3.8	20.3	6.3	3.3	0.4	6.0
Ta	0.39	0.43	0.11	0.09	0.08	0.19	0.14	0.25	0.34	0.22	0.83	0.46	0.20	0.03	0.30
Pb	6.4	8.6	11.0	4.6	6.5	7.2	9.4	7.6	3.7	4.9	11.7	6.7	162.0	8.2	5.1
Sr	283	124	588	68	185	191	244	430	559	102	447	310	421	256	176
Zr	67	77	19	80	52	64	34	45	71	56	161	62	63	18	79
Hf	1.80	2.10	0.51	2.10	1.30	1.60	1.03	1.40	2.78	1.53	3.70	1.70	1.87	0.70	1.40
La	8.67	7.38	9.38	3.81	2.46	10.68	4.94	9.49	24.64	9.66	36.19	8.42	9.83	2.12	1.64
Ce	21.58	17.85	18.83	9.79	6.90	24.71	11.86	24.02	70.20	21.27	80.21	19.42	22.07	5.66	5.94
Pr	3.26	2.42	2.19	1.45	1.15	4.14	1.55	3.54	10.20	2.52	8.91	2.80	2.82	0.85	1.06
Nd	15.01	11.33	9.16	7.49	6.02	12.93	7.21	15.99	46.45	9.84	31.46	12.99	12.41	3.99	5.32
Sm	4.66	3.18	2.06	2.86	2.14	3.08	2.00	4.22	10.34	2.04	5.98	3.73	3.23	1.17	2.01
Eu	1.33	1.34	0.82	1.06	0.84	0.90	0.51	1.27	2.76	0.69	1.61	1.36	1.08	0.61	0.74
Gd	4.89	3.38	1.60	4.08	2.77	3.11	2.01	4.22	8.85	2.31	4.92	4.31	3.10	1.46	2.21
Tb	0.79	0.55	0.20	0.76	0.48	0.50	0.32	0.69	1.20	0.35	0.76	0.74	0.51	0.26	0.37
Dy	4.65	3.48	1.09	5.18	3.10	2.87	2.16	4.19	7.93	2.25	4.18	4.35	3.51	1.74	2.31
Ho	0.97	0.71	0.23	1.15	0.66	0.63	0.46	0.88	1.60	0.46	0.86	0.90	0.76	0.40	0.49
Er	2.44	1.86	0.62	3.21	1.87	1.78	1.32	2.31	4.83	1.29	2.27	2.34	2.30	1.23	1.29
Tm	0.33	0.27	0.10	0.48	0.26	0.26	0.21	0.30	0.68	0.19	0.33	0.34	0.35	0.19	0.18

Table 3 (continued)

Rock type*	KyE	KyE	KyE	E	E	E	E	E	E	E	A	A	A	A	G
Area	CSGC	CSGC	CSGC	CSGC	CSGC	CSGC	CSGC	CSGC	CSGC	CSGC	CSGC	CSGC	SSGC	SSGC	CSGC
Sample	EM3	SP11	TN14	OP1	OP7	ZEH1	SP50	SP56	FU7	FE10	WO2	FE12	WEH2	GÖ2	LA41
Yb	1.97	1.82	0.65	2.91	1.70	1.73	1.19	1.91	4.61	1.27	2.05	2.06	2.37	1.31	1.12
Lu	0.29	0.27	0.10	0.44	0.27	0.25	0.16	0.29	0.66	0.22	0.33	0.28	0.36	0.21	0.18

*Ky-E = kyanite eclogite, E = eclogite, A = amphibolite without any eclogite relics, G = relic mafic granulite. n.a. = not analysed

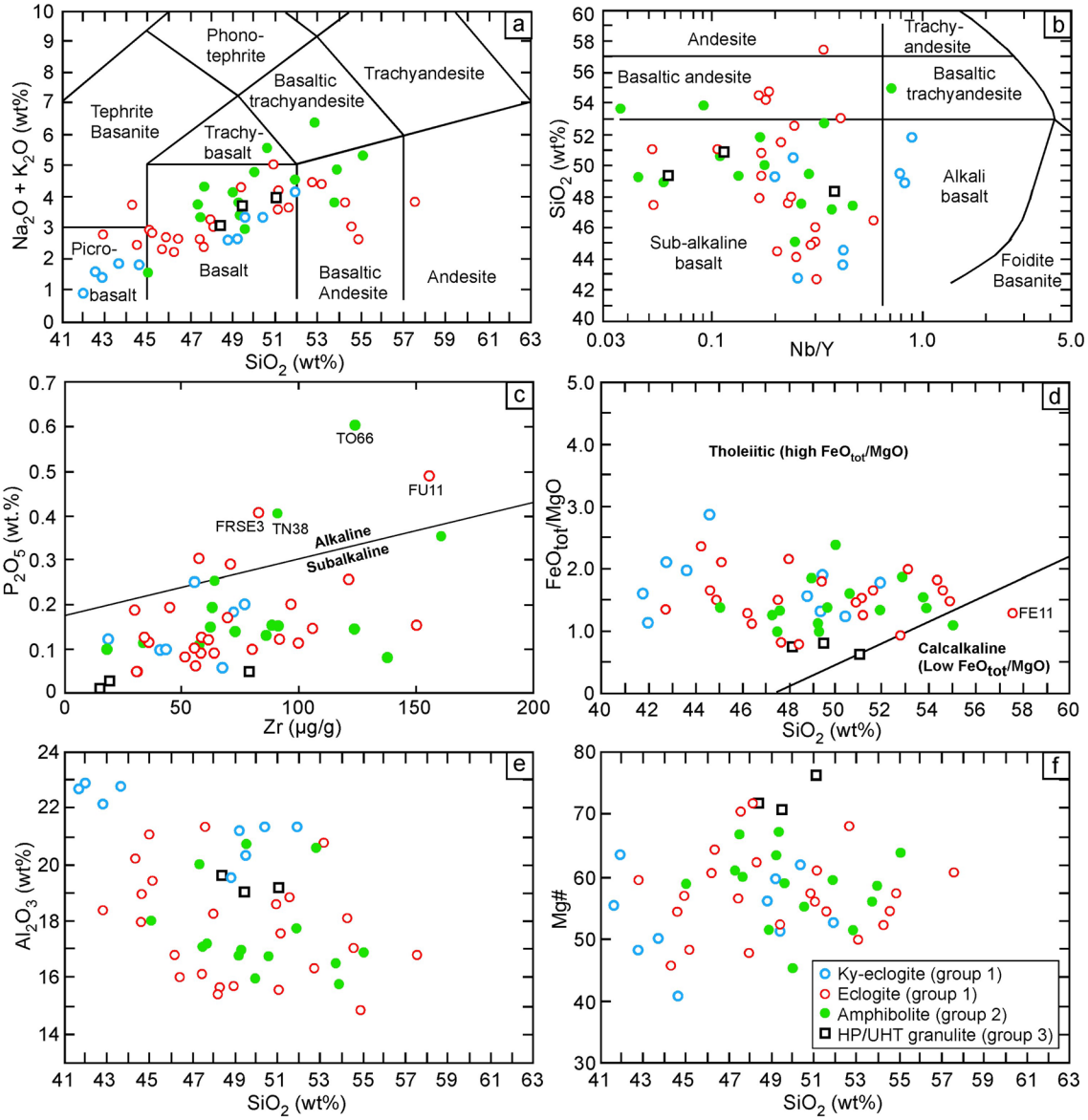

Fig. 5 Position of metabasites from the Schwarzwald in nomenclature diagrams. Eclogitic relics and amphibolites are given in red open circles, granulitic relics in green open squares. **a** Total alkalis vs silica (TAS) diagram after Le Maitre (2002). Most of the samples plot into the fields of basalt and basaltic andesite. **b** SiO_2 vs Nb/Y diagram after Winchester and Floyd (1977) showing the subalkaline character of the investigated metabasites. Note that the boundary between subalkaline basalt and basaltic andesite is at 53 wt % SiO_2, instead of 52 wt % as in **a**. **c** P_2O_5 vs Zr diagram discriminationg alkaline and subalkaline basalts (Winchester and Floyd, 1976). **d** FeO_{tot}/MgO vs SiO_2 for tholeiitic (high FeO_{tot}/MgO) and calcalkaline (low FeO_{tot}/MgO) basalts (Miyashiro 1975)

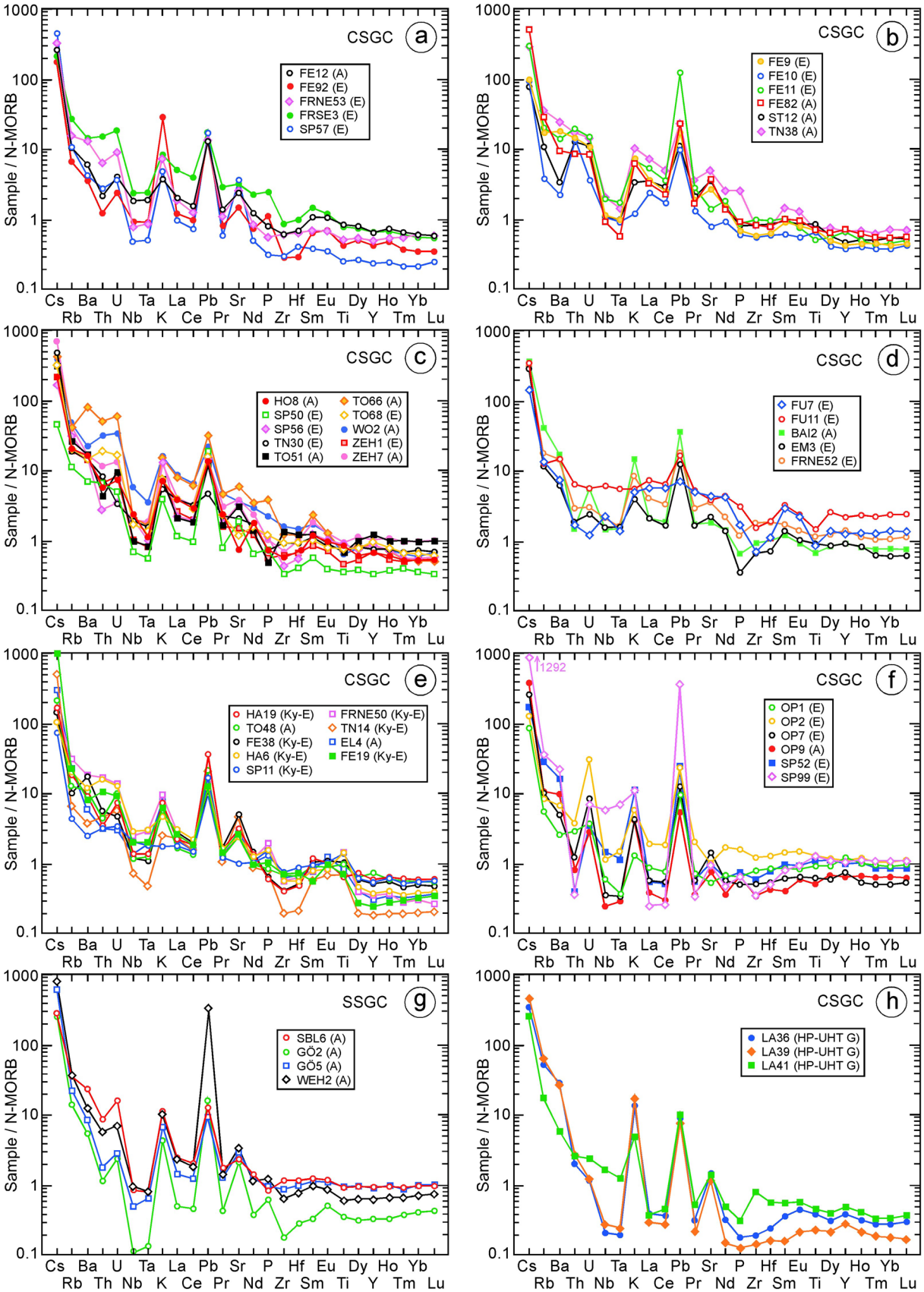
CSGC a
FE12 (A)
FE92 (E)
FRNE53 (E)
FRSE3 (E)
SP57 (E)
CSGC b
FE9 (E)
FE10 (E)
FE11 (E)
FE82 (A)
ST12 (A)
TN38 (A)
CSGC c
HO8 (A)
SP50 (E)
SP56 (E)
TN30 (E)
TO51 (A)
TO66 (A)
TO68 (E)
WO2 (A)
ZEH1 (E)
ZEH7 (A)
CSGC d
FU7 (E)
FU11 (E)
BAI2 (A)
EM3 (E)
FRNE52 (E)
CSGC e
HA19 (Ky-E)
TO48 (A)
FE38 (Ky-E)
HA6 (Ky-E)
SP11 (Ky-E)
FRNE50 (Ky-E)
TN14 (Ky-E)
EL4 (A)
FE19 (Ky-E)
CSGC f
11292
OP1 (E)
OP2 (E)
OP7 (E)
OP9 (A)
SP52 (E)
SP99 (E)
SSGC g
SBL6 (A)
GÖ2 (A)
GÖ5 (A)
WEH2 (A)
CSGC h
LA36 (HP-UHT G)
LA39 (HP-UHT G)
LA41 (HP-UHT G)
Sample / N-MORB
1000
100
10
1
0.1
Cs Ba U Ta La Pb Sr P Hf Eu Dy Ho Yb
Rb Th Nb K Ce Pr Nd Zr Sm Ti Y Tm Lu

◂**Fig. 6** N-MORB-normalized element concentration patterns of metabasite samples from different tectonic units of the central and southern Schwarzwald. Values of N-MORB are from Gale et al. (2013). While all samples are characterized by high concentrations of Cs, Rb and Ba, most samples show variable positive anomalies of the mobile elements K, Pb and Sr. Note that samples may have negative or positive anomalies of Zr-Hf. See text for further explanation

diagram of FeO_{tot}/MgO vs SiO_2 (Miyashiro 1975) (Fig. 5d), a tholeiitic nature of the basaltic protoliths is indicated. Concerning group 1 metabasites that suffered an eclogite-facies metamorphism, it is evident that nearly all Ky-bearing eclogites have CIPW-normative corundum (C). In the diagram of Al_2O_3 vs SiO_2 (Fig. 5e) the former Ky-bearing eclogites show the highest Al_2O_3 contents and there is no difference between the other three types of metabasites. For Mg# vs SiO_2 (Fig. 5f) there is no difference between the four different types.

In N-MORB normalized element concentration diagrams (Fig. 6) all samples of group 1 and 2 are characterized by variable positive Pb anomalies and nearly all samples show negative Nb–Ta, but positive K anomalies. There are only a few samples that show low K contents (e.g. FE10 in Fig. 6b, SP11 in Fig. 6e or FU11 in Fig. 6d). In general, the sizes of the positive anomalies of K and Pb are independent of each other. Moreover, many samples show positive Sr anomalies, but there are also samples with negative anomalies (e.g. FE10 and FE11 in Fig. 6b or OP1 and OP2 in Fig. 6f). Titanium and phosphorus contents are variable, with existing negative or positive anomalies, while Zr-Hf concentrations are either normal or show negative anomalies (e.g. FE92 in Fig. 6a or TN38 in Fig. 6b).

Chondrite (CI)-normalized (cn) REE patterns of group 1 and 2 metabasites (Fig. 7) are different concerning their $(La/Yb)_{cn}$ ratios and their Eu anomalies [$Eu/Eu^* = Eu_{cn}/(Sm_{cn} \times Gd_{cn})^{0.5}$]. While most samples show patterns with positive $(La/Yb)_{cn}$ values (1.10–13.5; Fig. 7a–e, g), some other samples have $(La/Yb)_{cn} < 1$ (Fig. 7f). Some samples (e.g. ZEH7, TO66, EM3) have significant negative Eu anomalies with Eu/Eu* values between 0.7 and 0.9 (Fig. 7c, d), others show positive anomalies with Eu/Eu* values of up to 2.06 (Fig. 7e). There is no systematic relationship between the values of Eu/Eu* and $(La/Yb)_{cn}$.

Samples of mafic metagranulites (group 3) are characterized by strongly positive K, Pb and Sr anomalies and negative P anomalies in N-MORB normalized element concentration diagrams (Fig. 6h). Furthermore, two of these samples (LA36, LA39) show marked negative Nb–Ta anomalies. Chondrite-normalized REE patterns of all three samples are relatively flat at low concentrations and show small, but significant positive Eu anomalies (Fig. 7h). The three samples show high Mg# values between 68.6 and 74.4 and Ni concentrations of 124–154 µg/g.

Discussion

Pressure–temperature conditions of granulite-facies metamorphism

The *P–T* evolution of the mafic granulites (group 3 metabasites) was first investigated in Hanel et al. (1993). Usage of Grt-Cpx, Grt-Opx and two-pyroxene thermometry and Grt-Opx-Pl-Qtz barometry resulted in assumed formation conditions of 1.0–1.1 GPa and 780–850 °C. These values are lower than those published for felsic granulites of the Schwarzwald. For these rocks, metamorphic conditions were estimated as 1.4–1.8 GPa and 950–1015 °C by Marschall et al. (2003). On the other hand, Zack et al. (2004) gave a Zr-in-rutile temperature of 980 °C (at 1.4 GPa) on one granulite from the CSGC. A more detailed analysis of the petrologic evolution of these rocks is in preparation.

Pressure–temperature conditions of eclogite-facies metamorphism and amphibolite-facies overprint

All metabasites of group 1, but possibly also those of group 2 that contain no relict eclogite-facies minerals, had an eclogitic history for which conditions of > 1.6 GPa and 670–750 °C have been proposed (Kalt et al. 1994b). However, former Al-rich eclogites contained kyanite I in coexistence with Cpx I that is characterized by jadeite contents of up to 47 mol % (Table 1). Using the reaction $Pg = Jd + Ky + H_2O$ as a geothermobarometer (Holland 1979) yields higher pressures of up to 2.0 GPa (at 670 °C) or 1.8 GPa (at 750 °C). Such pressure values correspond to depth values between 65 and 58 km, which then result in an average temperature-depth gradient of 10–13 °C/km. Such conditions plot between those of an average and a warm top-of-the-slab geotherm (Penniston-Dorland et al. 2015: Fig. 5f). It follows, that during subduction to a depth between 65 and 58 km, the metabasites were progressively dehydrated leading to a relatively dry eclogite assemblage of Grt I + Omp I + Rt I + Qtz I ± Ky I ± Ep I ± Amp I.

There exist a lot of calculated phase diagrams (pseudosections) for a range of MORB compositons (e.g. Rebay et al. 2010; Wei and Clarke 2011; Hernández-Uribe and Palin 2019; Wei and Duan 2019). These calculations show that resulting mineral assemblages are not only dependent on *P* and *T*, but also on H_2O content and oxidation state of the system. Moreover, chemical parameters such as X_{MgO} [= molar $MgO/(MgO + FeO_{tot})$] will also play an important role. In particular, at 2.0 GPa and 700 °C, the calculated mineral assemblage is strongly dependent on X_{MgO} (Wei and Clarke 2011). With increasing X_{MgO}, the calculated mineral assemblage changes from Grt + Omp + Ep ($X_{MgO} \leq 0.27$), via Grt + Omp + Ep + Ky

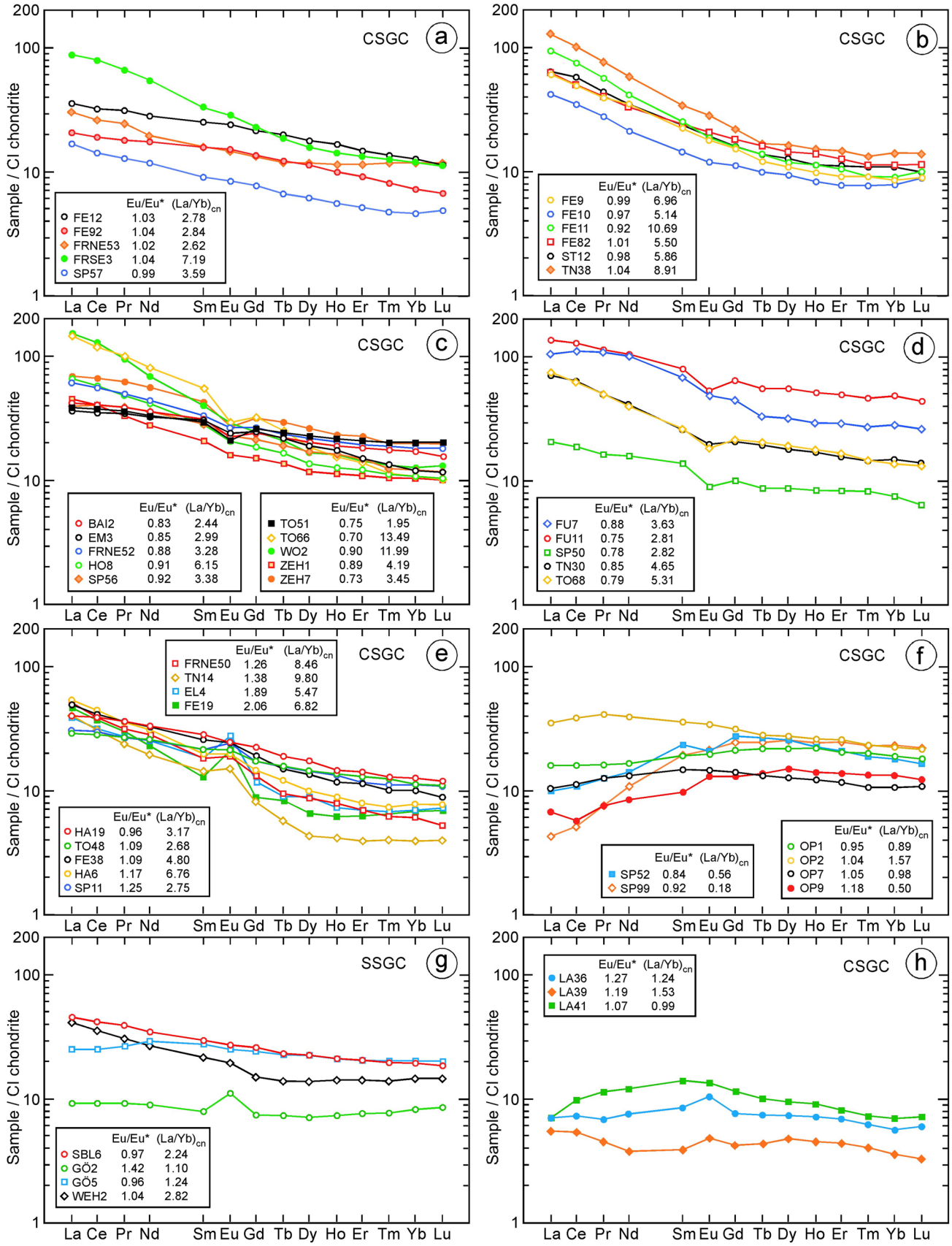
CSGC a
Eu/Eu* (La/Yb)cn
FE12 1.03 2.78
FE92 1.04 2.84
FRNE53 1.02 2.62
FRSE3 1.04 7.19
SP57 0.99 3.59
CSGC b
Eu/Eu* (La/Yb)cn
FE9 0.99 6.96
FE10 0.97 5.14
FE11 0.92 10.69
FE82 1.01 5.50
ST12 0.98 5.86
TN38 1.04 8.91
CSGC c
Eu/Eu* (La/Yb)cn
BAI2 0.83 2.44
EM3 0.85 2.99
FRNE52 0.88 3.28
HO8 0.91 6.15
SP56 0.92 3.38
Eu/Eu* (La/Yb)cn
TO51 0.75 1.95
TO66 0.70 13.49
WO2 0.90 11.99
ZEH1 0.89 4.19
ZEH7 0.73 3.45
CSGC d
Eu/Eu* (La/Yb)cn
FU7 0.88 3.63
FU11 0.75 2.81
SP50 0.78 2.82
TN30 0.85 4.65
TO68 0.79 5.31
CSGC e
Eu/Eu* (La/Yb)cn
FRNE50 1.26 8.46
TN14 1.38 9.80
EL4 1.89 5.47
FE19 2.06 6.82
Eu/Eu* (La/Yb)cn
HA19 0.96 3.17
TO48 1.09 2.68
FE38 1.09 4.80
HA6 1.17 6.76
SP11 1.25 2.75
CSGC f
Eu/Eu* (La/Yb)cn
SP52 0.84 0.56
SP99 0.92 0.18
Eu/Eu* (La/Yb)cn
OP1 0.95 0.89
OP2 1.04 1.57
OP7 1.05 0.98
OP9 1.18 0.50
SSGC g
Eu/Eu* (La/Yb)cn
SBL6 0.97 2.24
GÖ2 1.42 1.10
GÖ5 0.96 1.24
WEH2 1.04 2.82
CSGC h
Eu/Eu* (La/Yb)cn
LA36 1.27 1.24
LA39 1.19 1.53
LA41 1.07 0.99
Sample / CI chondrite
200
100
10
1
La Ce Pr Nd Sm Eu Gd Tb Dy Ho Er Tm Yb Lu

◂**Fig. 7** Chondrite-normalized REE patterns of metabasites from the central Schwarzwald (CI chondrite values are from McDonough and Sun 1995). Values of $(La/Yb)_{cn}$ and Eu/Eu* $[=Eu_{cn}/(Sm_{cn} \times Gd_{cn})^{0.5}]$ are given. **a** Samples with Eu/Eu* of ~ 1 and $(La/Yb)_{cn} > 1$. **b** Samples with $(La/Yb)_{cn} > 1$ and a negative Eu anomaly. **c** and **d** Samples with $(La/Yb)_{cn} > 1$ and a negative Eu anomaly. **e** Samples with $(La/Yb)_{cn} > 1$ and a positive Eu anomaly. **f** Samples with $(La/Yb)_{cn} < 1$ suggesting a MORB heritage. **g** Samples from the SSGC. **h** Mafic metagranulites showing patterns that suggest a cumulate nature of the protoliths

($X_{MgO} = 0.27–0.52$) and Grt + Omp + Ky ($X_{MgO} = 0.52–0.67$) to Grt + Omp + Amp + Ky ($X_{MgO} > 0.67$), whereby all assemblages contain Ph + Qtz + H_2O. Phengite, however, may only be present, if the subducted MORB is altered and contains enough K.

During subduction, the more or less hydrated mafic rocks lose their porosity by compaction, and pore fluids will be expelled. As a consequence, nearly all of the remaining H_2O will be bound in hydrous minerals. With the increasing metamorphic grade, possible H_2O-bearing phases in metabasites are prehnite, pumpellyite, chlorite, epidote, amphibole, paragonite, phengite, and eventually also Mg-chloritoid. Their modal fractions will, to a large degree, control the remaining H_2O content of the rock. Most of the aqueous fluid produced by dehydration reactions could be lost along with localized fracture systems (e.g. Zack and John 2007; Klemd 2013; Plümper et al. 2017). At about 2.0 GPa and 700 °C, low H_2O contents will favour the eclogite assemblage of Grt + Omp + Rt + Qtz ± Ep ± Amp (e.g. Rebay et al., 2010; Hernández-Uribe and Palin 2019; Wei and Duan 2019). Moreover, saline solutions, if present during subduction of the metabasites, will cause dehydration reactions to proceed at lower temperatures and shallower depth compared to pure H_2O fluids.

After their formation, the eclogites with their country rocks were exhumed from a depth of about 65 km to the middle crust (~ 15 km depth). Relative to their ductile quartz-rich country rocks, the eclogites were more brittle and this quality delayed their retrograde evolution. Increasing a_{H2O} then caused the reaction to amphibolite-facies mineral assemblages at about 0.4–0.5 GPa and 675–690 °C (Mehnert and Büsch 1982; Kalt et al. 1994a, b).

The fact, that sapphirine was formed within the symplectites after kyanite, does not necessarily imply that temperatures were higher than ~ 700 °C. The lower thermal stability limit of Fe-free sapphirine of compositions 2:2:1 and 7:9:3 ($MgO:Al_2O_3:SiO_2$) at a pressure of 0.7 GPa was determined as ~ 750 °C by Seifert (1974). For Fe^{2+}-bearing sapphirine this lower thermal stability limit should be located at even lower temperatures.

According to the experimental phase-equilibrium study of Al- and Ti-contents of calcic amphiboles in a MORB system by Ernst and Liu (1998), amphibole compositions may be used as a semiquantitative thermobarometer. While Al_2O_3 contents in Ca-amphibole increase with both *P* and *T*, TiO_2 isopleths are nearly independent of pressure and show increasing TiO_2 contents with an increase in temperature. Amphibole II compositions are characterized by very low concentrations of TiO_2 (< 0.4 wt %) and high values (> 12 wt %) of Al_2O_3 (Table 1). In equilibrium, such amphibole compositions would indicate unrealistic *P–T* conditions of ~ 2–3 GPa and ~ 500 °C. It is clear, however, that Amp II was formed in local environments with bulk compositions unlike that of MORB. Therefore, compositions of Amp II cannot be used to deduce the *P–T* conditions at which they were formed. In marked contrast, Amp III compositions show TiO_2 contents of ~ 0.9 wt % and Al_2O_3 contents of ~ 8 wt % (Table 1) suggesting *P–T* conditions of about 0.5 GPa and 680 °C (Ernst and Liu 1998: Figs. 8 and 9) that are very similar to those suggested for the anatexis of the gneisses in which the amphibolites are hosted (0.4–0.5 GPa / 675–690 °C; Mehnert and Büsch 1982).

Metasomatism during metamorphic evolution

The metabasites of the CSGC and SSGC form small mafic bodies included within plagioclase-biotite gneisses that are poor in K-feldspar and were probably formed from continent-derived flyschoid sediments such as greywackes. In such a tectonic environment (trench), different types of basaltic rocks can occur in intimate primary, but also in secondary association with flyschoid sediments. First of all, these are orogenic basalts, such as back-arc basin basalts (BABB), island-arc tholeiites (IAT) or calc-alkaline basalts (CAB). All these rocks are generated above subduction zones, but blocks of them may later be included in the trench sediments. Secondly, there is the subducting oceanic crust that may include a wide range of chemical compositions from normal or enriched mid-ocean ridge basalt (N-MORB, E-MORB) to ocean island basalt (OIB). All these rocks may have been affected by seafloor alteration and hydrothermal metamorphism.

If the metabasic rocks of group 1 and 2 as well as those of group 3 in the CSGC and SSGC are derived from oceanic basalts (e.g. MORB, BABB or IAT), their chemical compositions might have been successively influenced by (1) submarine hydrothermal alteration, (2) subduction-zone metamorphism and related fluid-rock interactions, (3) fluid activity during L*P*-H*T* metamorphism (amphibolitization), and (4) hydrothermal activity within the crust during late to post-Variscan times. During all these processes, the extent of element mobility will strongly depend on the predominant physicochemical conditions, that is to say, the *P–T* conditions and the compositions of the aqueous (solute-poor or solute-rich) fluids that are coexisting, but not necessarily

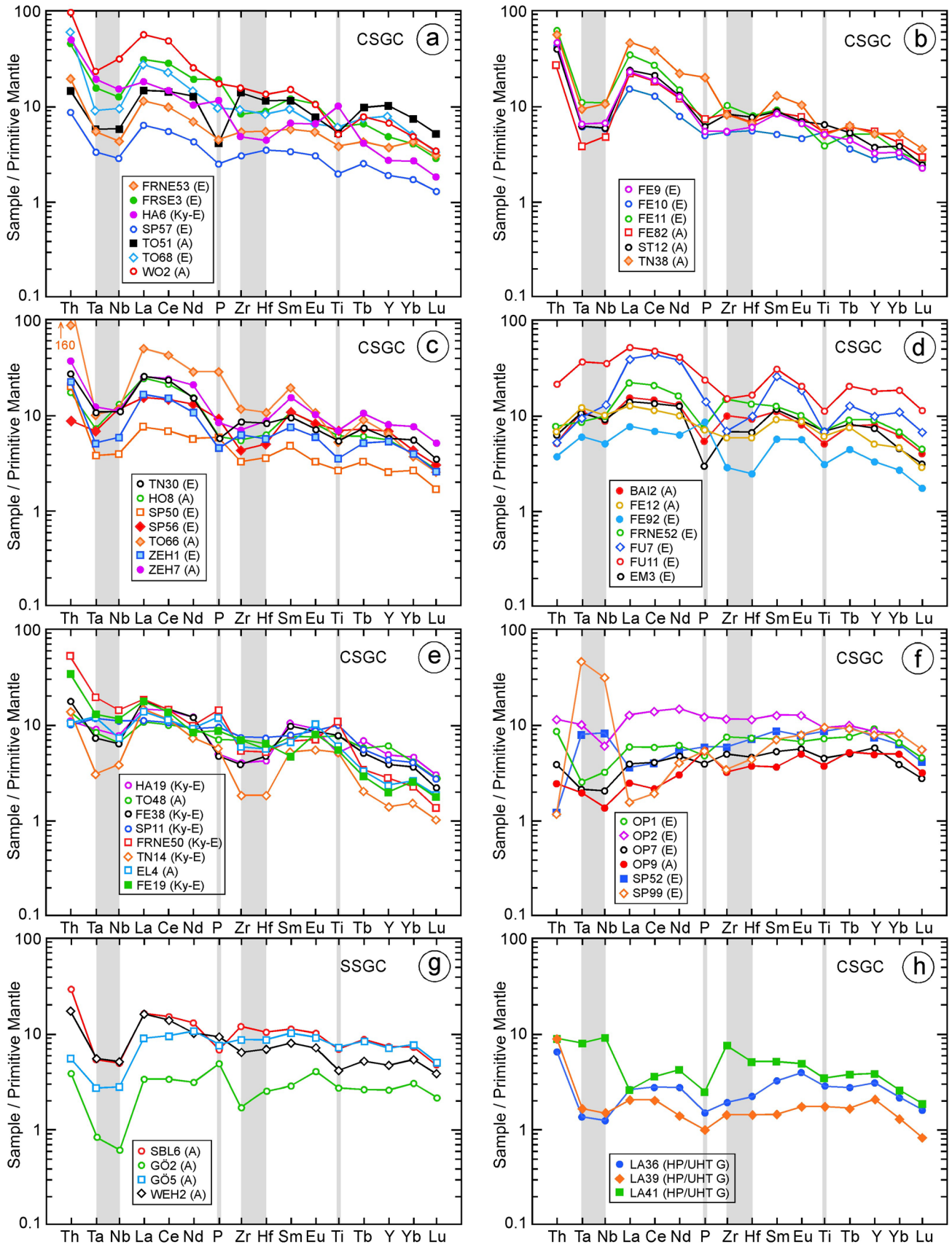
CSGC a
FRNE53 (E)
FRSE3 (E)
HA6 (Ky-E)
SP57 (E)
TO51 (A)
TO68 (E)
WO2 (A)
CSGC b
FE9 (E)
FE10 (E)
FE11 (E)
FE82 (A)
ST12 (A)
TN38 (A)
CSGC c
160
TN30 (E)
HO8 (A)
SP50 (E)
SP56 (E)
TO66 (A)
ZEH1 (E)
ZEH7 (A)
CSGC d
BAI2 (A)
FE12 (A)
FE92 (E)
FRNE52 (E)
FU7 (E)
FU11 (E)
EM3 (E)
CSGC e
HA19 (Ky-E)
TO48 (A)
FE38 (Ky-E)
SP11 (Ky-E)
FRNE50 (Ky-E)
TN14 (Ky-E)
EL4 (A)
FE19 (Ky-E)
CSGC f
OP1 (E)
OP2 (E)
OP7 (E)
OP9 (A)
SP52 (E)
SP99 (E)
SSGC g
SBL6 (A)
GÖ2 (A)
GÖ5 (A)
WEH2 (A)
CSGC h
LA36 (HP/UHT G)
LA39 (HP/UHT G)
LA41 (HP/UHT G)
Sample / Primitive Mantle
100
10
1
0.1
Th Ta Nb La Ce Nd P Zr Hf Sm Eu Ti Tb Y Yb Lu

◂**Fig. 8** Primitive mantle-normalized element concentration patterns for nearly immobile elements. **a** and **b** Patterns with a clear negative Nb–Ta anomaly (relative to Th and La) and variable normalized element concentrations of P, Zr-Hf and Ti. **c** Patterns with a negative Nb–Ta and a positive Eu anomaly. **d** Samples with low Th contents and variable concentrations of P, Zr-Hf and Ti. **e** Samples with a negative Nb–Ta and Zr-Hf anomalies. **f** Samples that show a minor negative (OP) or a positive (SP) Nb–Ta anomaly. **g** Samples from the SSGC show negative Nb–Ta anomalies and variable contents of Zr-Hf, P and Ti. **h** Patterns of three metagranulite samples with different behavior of Nb–Ta. See text for further explanation

in equilibrium with the solid phases and possibly small amounts of melt.

In case that the investigated metabasites initially suffered complex multistage hydrothermal alteration and submarine weathering, these processes must have had variable chemical effects. Seawater-basalt reactions often start at high temperature during the cooling of the newly created lithosphere (e.g. Jarrard 2003; Alt et al. 2010) and then proceed at lower temperatures during the lifetime of the oceanic crust. These reactions depend on local physicochemical conditions, e.g. temperature, oxygen and sulfur fugacities, chemical compositions of involved fluids, and water/rock ratio. There are a lot of studies on different parts of altered oceanic crust, and the chemical picture of these processes is still complicated and far from being uniform (e.g. Staudigel et al. 1996; Bach et al. 2003; Kelley et al. 2003; Schramm et al. 2005; Staudigel 2014). Still, there is a broad consense that (1) the contents of Si and Ca are often decreased, while that of Mg is increased, and (2) LILE (Cs, Rb, Ba, K, Pb) and U are often enriched in the altered rocks, while other elements, such as Sr, will either be enriched or depleted. Such alterations are often spatially limited and chemically heterogeneous. For example, in a vertical profile of the oceanic crust (Hole 504B), K_2O was found to increase irregularly from an original value of about 0.04 wt % below ~ 600 m sub-basement to a range of values (0.04–0.45 wt %) near to the surface of the oceanic crust (Jarrard 2003), and in each sample such an increase in K is not always accompanied by a similar percentage of increase in other LILE or U.

Partial dehydration of the subducted metabasic rocks of the Schwarzwald occurred below the *P–T* conditions at which they were transformed to eclogites, i.e. below ~ 2.0 GPa and 670–750 °C, corresponding to depth values of less than 65 km. At these conditions, that are far below those of the second critical endpoint in the system MORB + H_2O (Kessel et al. 2005a, b; Mibe et al. 2011), the solubility of most elements in aqueous fluids is fairly low, unless the fluids contain relatively high amounts of saline components, such as chlorine or fluorine. Such components have experimentally been shown to strongly increase fluid/solid partition coefficients for LILE (Cs, Rb, Ba, K, Pb), Th, U, and LREE, but not those for HREE and HFSE (Kessel et al. 2005a, b; Bali et al. 2011; Kawamoto et al. 2014; Tsay et al. 2014, 2017; Keppler 2017; Rustioni et al. 2019). During subduction, pore fluids (with Cl, F) in the altered oceanic crust will be lost at shallow depths (less than ~ 5 km), i.e. before relevant (OH, Cl, F)-bearing solid phases such as chlorite, epidote, amphibole or apatite become unstable (Jarrard 2003; Barnes et al. 2018). During further subduction, a number of dehydration reactions will take place and will be combined with a further bulk-rock loss in Cl and F. The last dehydration reactions that probably took place in the investigated rocks were those by which the contents of amphibole and epidote were minimized. It is worth mentioning, that serpentine, that might have been in tectonic contact with the eclogites, has its maximum thermal stability at about 2.2 GPa/720 °C (Ulmer and Tromssdorff 1995), i.e. somewhat above the *P–T* conditions at which the eclogites were formed.

As a consequence, it follows that the devolatilization of the investigated metabasites during subduction was probably accompanied by a significant impoverishment in those mobile elements that had probably been gained during submarine hydrothermal alteration.

Stages II and III in the evolution of the investigated metabasites include their uplift to about 15 km depth and their retrograde partial or complete transformation from eclogite to amphibolite. The chemical effects of this amphibolitization can best be evaluated by looking first at eclogite samples that were only moderately altered and do not contain significant amounts of amphibole, plagioclase or even biotite. Only five of our samples (FE10, FU7, FU11, SP11, TN14) are in accordance with this condition. These samples show relatively low K_2O contents (0.18–0.78 wt%) and have low K/La and K/Th ratios, but high N-MORB normalized Th/U ratios (Fig. 6b, d, e). Moreover, the size of the positive Pb-anomaly is variable and independent of the behavior of K and U. We conclude that the LILE (Cs, Rb, Ba, K, Pb) and U were strongly, but variably re-enriched during amphibolite-facies retrogression of the eclogites. Most probably, this was also true during later hydrothermal alteration events, such as the widespread sericitization of plagioclase. We do, however, not assume that elements such as Th and the LREE were significantly mobile during these alterations. There is only one sample (OP2) that may have lost some La and Ce, and another sample (OP9) that shows a negative Ce anomaly (Fig. 7f).

Parental igneous rocks of the metabasites from the Schwarzwald

Since we have to accept that the concentrations of LILE were drastically increased during and after the L*P*-H*T* metamorphism leading to a partial or complete amphibolitization of the metabasites, we will not use these strongly mobile

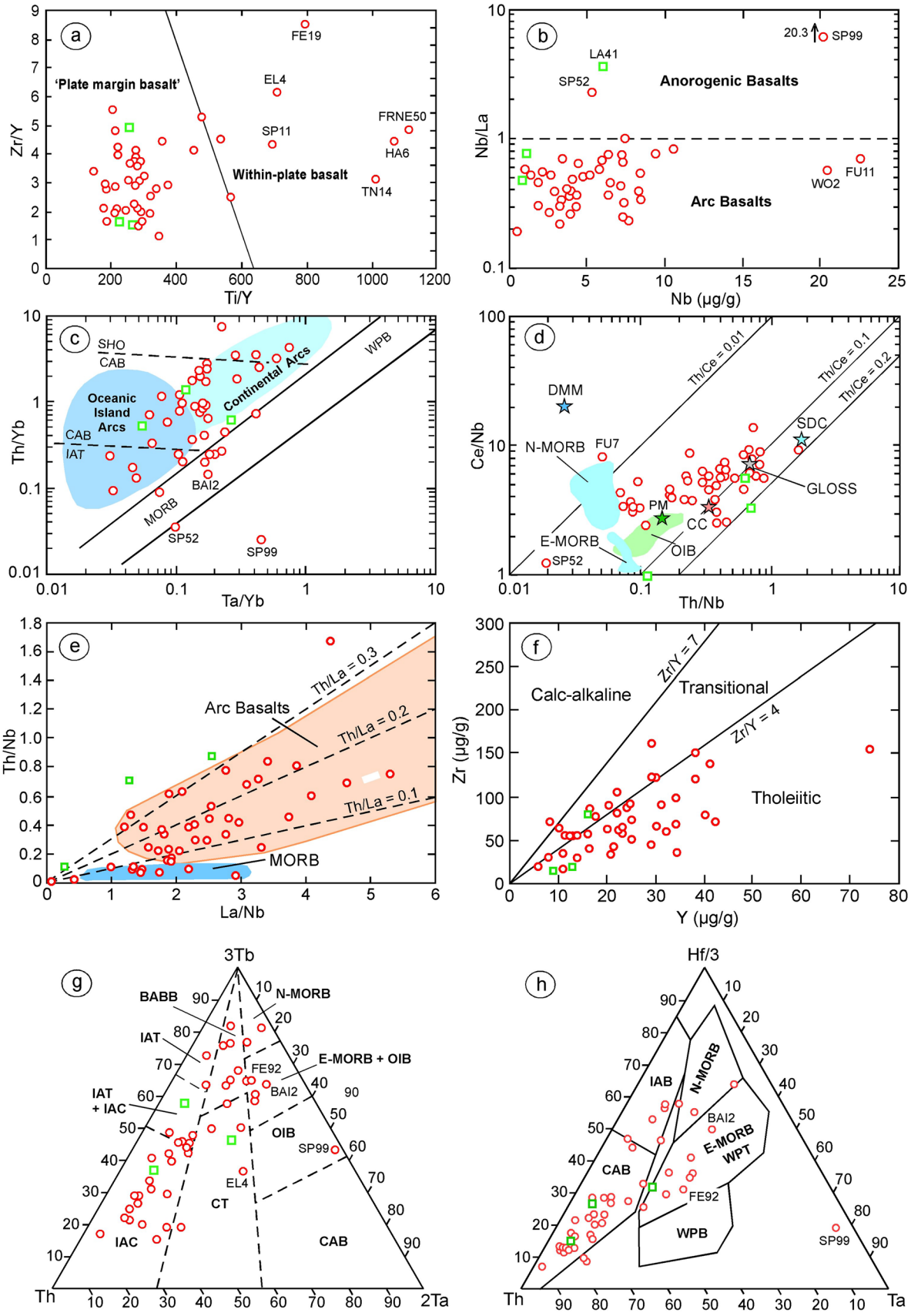
a
'Plate margin basalt'
Within-plate basalt
FE19
EL4
SP11
FRNE50
HA6
TN14
Zr/Y
Ti/Y
b
Anorogenic Basalts
Arc Basalts
LA41
SP52
20.3
SP99
WO2
FU11
Nb/La
Nb (µg/g)
c
SHO
CAB
Oceanic Island Arcs
CAB
IAT
Continental Arcs
WPB
BAI2
MORB
SP52
SP99
Th/Yb
Ta/Yb
d
DMM
N-MORB
FU7
Th/Ce = 0.01
Th/Ce = 0.1
Th/Ce = 0.2
SDC
GLOSS
PM
CC
E-MORB
SP52
OIB
Ce/Nb
Th/Nb
e
Arc Basalts
Th/La = 0.3
Th/La = 0.2
Th/La = 0.1
MORB
Th/Nb
La/Nb
f
Calc-alkaline
Transitional
Tholeiitic
Zr/Y = 7
Zr/Y = 4
Zr (µg/g)
Y (µg/g)
g
3Tb
BABB
N-MORB
IAT
E-MORB + OIB
FE92
BAI2
IAT + IAC
OIB
SP99
EL4
CT
IAC
CAB
Th
2Ta
h
Hf/3
IAB
N-MORB
BAI2
E-MORB
WPT
CAB
FE92
WPB
SP99
Th
Ta

◂**Fig. 9** Various basalt discrimination diagrams applied for metabasaltic rocks from the Schwarzwald (red symbols = group 1 and group 2; green symbols = group 3). **a** Zr/Y vs Ti/Y diagram discriminating basalts from convergent plate margins and within-plate basalts (Pearce and Gale, 1977). **b** Nb/La vs Nb diagram discriminating anorogenic from arc basalts (Xia and Li, 2019). **c** Th/Yb vs Ta/Yb diagram (Pearce 1982). Most of the samples clearly plot above the trend of anorogenic oceanic basalts (MORB to WPD = within plate basalt) and are clearly orogenic. **d** Ce/Nb vs Th/Nb diagram (Saunders et al. 1988). Fields for N-MORB, E-MORB and OIB and points of depleted MORB mantle (DMM), primitive mantle (PM), continental crust (CC), global subducting sediment (GLOSS) and slab-derived component (SDC) are from Wang et al. (2019). **e** Th/Nb vs La/Nb diagram after Plank (2005). MORB basalt is characterized by very low Th/Nb ratios, while arc basalts generally show elevated ratios. **f** Diagram of Zr vs Y, modified after Lentz (1998), to distinguish between calc-alkaline, transitional and tholeiitc basalts. **g** Triangular Th-3 Tb-2Ta discrimination diagram after Cabanis and Thiéblement (1988) with compositional fields of back-arc basin basalts (BABB), continental alkali basalts (AB), continental tholeiites (CT), island arc tholeiites (IAT), island arc calc-alkaline basalts (IAC), and ocean island basalts (OIB). **h** Th-Hf/3-Ta discrimination diagram after Wood (1980) with compositional fields of island-arc basalts (IAB), continental arc basalts (CAB), within-plate basalts (WPB) and within-plate tholeiites

elements in our attempt to identify parental volcanic rock types. Following Xia and Li (2019), we will instead restrict us to the abundances of the incompatible elements Th, Ta, Nb, La, Ce, Nd, P, Zr, Hf, Sm, Eu, Ti, Tb, Y, Yb, and Lu, normalized to the primitive mantle (McDonough and Sun 1995).

First of all, we have to interpret the chondrite-normalized REE spectra of the former kyanite eclogites (Fig. 7e). Except for sample HA19, these samples show positive Eu anomalies that are best explained by an accumulation of magmatic plagioclase. Therefore, these samples were possibly part of a gabbroic fractionation series. It is important to note, that within this group, there is one sample (EL4) that is completely recrystallized to an ordinary amphibolite.

Most samples show negative Ta-Nb anomalies relative to Th and La (Fig. 8). There are only a few exceptions to this 'rule'. Seven samples (Fig. 8d) are characterized by normalized Ta and Nb values that are higher than those of Th, but somewhat lower than those of La. Furthermore, two samples (SP52, SP99) show anomalously high Nb–Ta contents, i.e. they are depleted in La, Ce and Th, but have positive Nb–Ta anomalies (Fig. 8f). The other HFSE (Zr, Hf, Ti, P) behave somewhat unsystematic. Many samples show negative Zr-Hf anomalies (Fig. 8b, c, e), while Ti and P may have negative or positive anomalies. All these features, predominantly the negative Ta-Nb anomalies in combination with the variable behavior of P, Zr-Hf and Ti are typical features of orogenic basalts such as island-arc tholeiites (IAT) or calc-alkaline basalts (CAB). For more details, see Schmidt and Jagoutz (2017). We will now check this presumption by looking at more traditional discrimination diagrams.

In the diagram of Zr/Y vs Ti/Y (Fig. 9a), developed by Pearce and Gale (1977) to distinguish basalts from convergent plate margins from within-plate basalts, most of the investigated metabasites fall into the field of rocks from convergent plate margins. Some of the samples plot into the field of within-plate basalts and all these samples have positive Ti anomalies (relative to Sm) in primitive mantle-normalized incompatible trace element diagrams, for example, HA6 (Fig. 8a) or FRNE50 and SP11 (Fig. 8e).

The diagram Nb/La vs Nb (Fig. 9b) was successfully used by Xia and Li (2019) to discriminate between arc and anorogenic basalts. The data of most metabasites show Nb/La ratios smaller than unity suggesting an origin as arc basalts.

The frequently used diagram to distinguish arc from anorogenic basalts by looking at the relation of Th/Yb vs Ta/Yb (Fig. 9c) was developed by Pearce (1982). Again, most samples of the investigated metabasalts plot into the area of arc basalts. However, samples SP52 and SP99 that are both characterized by positive Nb–Ta anomalies (Fig. 8f) plot far outside the fields of arc basalts (Fig. 9c).

The diagram of Ce/Nb vs Th/Nb (Fig. 9d) is thought to be nearly independent of fractional crystallization of basalts (Saunders et al. 1988) and was used to discriminate between different types of basalt. In this diagram, the investigated metabasites form an array from the fields for N-type MORB via the points of continental crust to the compositions of typical subduction-related island-arc and continental arc basalts. A similar message is send by the diagram of Th/Nb vs La/Nb (Fig. 9e) from Plank (2005) that discriminates between anorogenic basalts that are derived from the depleted upper mantle (MORB) with low values of Th/Nb (mostly < 0.1) from those of arcs containing a continental sedimentary component (Th/La = 0.1–0.3). Almost all of the investigated metabasites have Th/La ratios that suggest an origin from arc basalts.

The diagram of Zr vs Y (Fig. 9f) was originally developed as a diagram of Zr/TiO_2 vs Y/TiO_2 by Lentz (1998) who used such a diagram to differentiate between metabasites that originiated from calc-alkaline basalts with $Zr/Y > 7$ from those with a tholeiitic heritage ($Zr/Y < 4$. Some authors have, however, slightly changed these boundaries (e.g. Ross and Bédard 2009), but we will use the original version. All investigated metabasites from the Schwarzwald show Zr/Y ratios between 1.05 and 8.57 and most samples have Zr/Y values below 4, suggesting a tholeiitic to transitional calc-alkaline/tholeiitic character of their protoliths.

In addition, there exist some triangular diagrams for differentiating the protoliths of metabasalts. In the diagram Th–3 Tb–2Ta after Cabanis and Thiéblement (1988), most of the samples plot into the fields of island-arc calc-alkaline basalts (IAC), island-arc tholeiites (IAT) and back-arc basin basalts (BABB) with transitions to MORB (Fig. 9g). Only one sample (SP99) that has a positive peak for Nb–Ta in a

primitive mantle-normalized concentration diagram (Fig. 8f) falls into the field of ocean-island basalts.

The diagram Th–Hf/3–Ta of Wood (1980) is perhaps the most used plot to distinguish basaltic rocks from different tectonic settings (Fig. 9h). Most of the Schwarzwald metabasites plot into the fields of arc basalts. Some samples, however, fall into the field of E-MORB and within-plate basalts (WPT). One sample (again SP99) falls exceptionally near the Ta corner.

Summarizing, we may state that the metabasic rocks are most probably derived from island-arc tholeiites and BABB. Some samples, however, might also have MORB precursors. It is important to note, that unlike many IAT and BABB, the metabasic rocks are characterized by very high Cs/Rb ratios, suggesting a metasomatic addition of aqueous fluid-mobile Cs to these rocks.

Possible equivalents of the investigated metabasites in other parts of the European Variscides

The Moldanubian Zone of the Central European Variscides exposed in the French Massif Central (FMC), the Vosges Mts (VM) and the Bohemian Massif (BM) contain at least two major tectonic units, the names of which vary from region to region. The uppermost 'Granulite (Gföhl) Unit' or 'Upper Gneiss Unit (UGU)' in the FMC consists of relic H*P*-UH*T* granulites with intercalations of UH*P*-UH*T* garnet-bearing peridotites and eclogites (e.g. Fuchs 1976; Thiele 1984; Rey et al. 1992; Gardien et al. 1997; Berger et al. 2010; Faryad et al. 2013; Altherr and Soder 2018; Sorger et al. 2020; Vanderhaeghe et al. 2020). Not only the garnet peridotites and eclogites but also the granulites of this unit locally contain relic UH*P* minerals such as coesite and diamond (Lardeaux et al. 2001; Naemura et al. 2011; Perraki and Faryad 2014; Jedlicka et al. 2015; Thiéry et al. 2015). It follows, that present-day H*P*-UH*T* granulites are most probably retrograded UH*P*-UH*T* felsic rocks.

In the Schwarzwald, the metabasites with a H*P*-UH*T* granulite heritage from north of Hohengeroldseck Castle can easily be connected with felsic H*P*-UH*T* metagranulites from the CSGC and SSGC described by Marschall et al. (2003). In the Vosges Mts, such rocks occur in close association with UH*P*-UH*T* garnet peridotites and such an association is typical for the 'Granulite (Gföhl) Unit' of the Moldanubian part of the BM (Altherr & Soder 2018). The fact that granulites from these two areas suffered severe retrogression has limited the interest to discover UH*P* phases in these rocks.

The lowermost 'Monotonous Unit' or 'Lower Gneiss Unit (LGU)' in the FMC consists of anatectic gneisses (mostly poor in K-feldspar) with intercalated small bodies of H*P*-H*T* eclogite and spinel peridotite. The rocks of this unit first suffered a H*P*-H*T* event that was followed by a L*P*-H*T* metamorphism, creating retrogressed eclogites surrounded by anatectic gneisses. At least all the metabasites from the Schwarzwald that contain eclogitogenic relics belong to this unit. The *P–T* conditions at which these eclogites were equilibrated can be narrowed down to ~ 2.0 GPa and 670–700 °C (this paper) and are thus nearly similar to those from the 'Monotonous Unit' of the BM (Faryad et al. 2013).

It is important to note that retrogressed eclogites also occur in the Böllsteiner Odenwald that forms part of the Mid-German Crystalline High. These eclogites were formed at *P–T* conditions (Will and Schmädicke 2001) that are similar to those at which the eclogites from the Schwarzwald were equilibrated. For these rocks Scherer et al. (2002) report Lu–Hf Grt-WR ages around the Famenian/Tournaisian boundary (~ 358 Ma). A paper with U–Pb ages (SIMS) of zircon from retrogressed eclogites of the Schwarzwald is in preparation (Hanel et al., unpubl. data).

Being aware that the two major units of the Moldanubian zone ('Monotonous Unit' and 'Granulite (Gföhl) Unit') are very similar in the Variscan chain of Central Europe (FMC, Vosges Mts, Schwarzwald, BM), it stays the problem of the plate tectonic setting by which these units were generated. Franke et al. (2017) argue for two subduction zones with opposite vergence underneath Bohemia (S-Armorica). These authors assume that the Saxothuringian Ocean was subducted to the SE, while the Galicia-Moldanubian Ocean was subducted to the NE as indicated by the Moravo-Silesian unit that was overthrust by the Moldanubian. Such a configuration, however, is hardly able to explain the presence of the two subduction-related units ('Monotonous Unit' with Eclogites metamorphosed at ~ 2 GPa and 670–700 °C, and 'Granulite (Gföhl) Unit' metamorphosed at ≥ 4 GPa and 950–1030 °C). Exhumation of such units normally occurs onto the lower plate, yet these units are part of the upper plate.

Conclusions

In the Moldanubian Schwarzwald, two large gneiss complexes are tectonically separated by the BLZ. In both gneiss complexes, metabasic rocks occur as small inclusions (< 800 m in diameter) within amphibolite-facies plagioclase-biotite gneisses of predominantly greywacke compositions. The rocks of these complexes suffered at least two major metamorphic events, the last of which was an allochemical amphibolite-facies overprint at 0.4–0.5 GPa / 675–690 °C and high water activities, which led to anatexis in gneisses with suitable compositions. The preceding high-pressure metamorphic event is predominantly documented in metabasic rocks. Most of these contain mineral relics (garnet, omphacite, rutile, ± kyanite) of an earlier eclogite-facies metamorphism at 2.0 GPa and

670–700 °C. The thermal gradient during high *P*/*T* metamorphism thus was 10–13 °C/km, corresponding to an average to warm top-of-the-slab geotherm. Locally, however, there are metabasites that were metamorphosed during a H*P*-UH*T* granulite-facies event (1.5–2.0 GPa/950–1000 °C), before they were overprinted by the later amphibolite-facies metamorphism. Finally, there are amphibolites without any relics of a former H*P*-H*T* or H*P*-UH*T* metamorphism.

In this study, we investigated the chemical compositions of all these metabasic rocks. We found no systematic differences between samples from the three groups. In general, the rocks underwent strong metasomatism during and after the second metamorphic event, the amphibolite-facies metamorphism with beginning anatexis. Elements such as LILE (Cs, Rb, Ba, K, Pb, ± Sr) and U, which are highly soluble in aqueous fluids, were introduced to the rocks in variable proportions. Elements with lesser mobility, such as REE and HFSE were not significantly changed. Thorium might have been mobile in some samples showing low Th/La ratios.

The first event that the metabasites might have undergone was submarine alteration and/or hydrothermal metamorphism, eventually leading to an increase in LILE and U as well as changes in the relative amounts of Si, Mg, Fe, Ca, and Na. We, therefore, did not use all these potentially mobile elements for the determination of the primary volcanic rocks.

During subduction (groups 1 and 2) or during granulite-facies metamorphism (group 3), the rocks became strongly dehydrated under elevated *P*–*T* conditions. Most of our samples were transformed to eclogites that were almost free of OH-bearing phases such as amphibole or epidote. We, therefore, assume that the chemical budgets of such nearly dry eclogite samples did not contain large amounts of LILE and U that are well solvable in aqueous fluids liberated during high *P*/*T* metamorphism leading to eclogitization.

Chemical discrimination diagrams based on elements such as Th, HFSE, REE, and Y, that are largely immobile in aqueous fluids at *P*–*T* conditions below 2 GPa and 800 °C, strongly suggest that the former basaltic/andesitic rocks (groups 1–3) were island arc tholeiites, back-arc basin basalts and MORB.

Supplementary Information The online version contains supplementary material available at https://doi.org/10.1007/s00531-021-02016-w.

Acknowledgements Klaus Fesenmeier (University of Freiburg), Ilona Fin and Oliver Wienand (Heidelberg University) prepared the thin sections. Heinrich Taubald (University of Tübingen) carried out the XRF analyses for major elements. Dieter Garbe-Schönberg (University of Kiel) and Helene Brätz (University of Erlangen-Nürnberg) performed trace element analyses by LA-ICP-MS. Hans-Peter Meyer assisted with the microprobe work (calibration) and with formula calculations. Constructive discussions with Angelika Kalt, Wolfhard Wimmenauer, Rainer Groschopf and Hiltrud Müller-Sigmund are gratefully acknowledged. Furthermore, we thank Dejan Prelević and, in particular, Dominik Sorger for their careful reviews and suggestions. This research did not receive any specific grant from funding agencies in the public, commercial, or non-for-profit sectors.

Authors' contributions RA suggested this study, participated in parts of the field work and drafted the manuscript. During their Dr. rer. nat. theses, SH and HK carried out most of the field and petrographic work and parts of the bulk-rock analyses. MH contributed by work at the electron scanning microscope. All authors read and approved the final manuscript.

Funding Open Access funding enabled and organized by Projekt DEAL. This research did not receive any specific grant from funding agencies in the public, commercial, or non-for-profit sectors.

Declarations

Coflict of interest The authors declare that they have no known competing financial interests or personal relationships that coul have appeared to influence the work reported in this paper.

References

Alt JC, Laverne C, Coggon RM, Teagle DAH, Banerjee NR, Morgan S, Smith-Duque CE, Harris M, Galli L (2010) Subsurface structure of a submarine hyrothermal system in ocean crust formed at the East Pacific Rise, ODP/IODP Site 1256. Geochem Geophys Geosyst 11:Q10010. https://doi.org/10.1029/2010GC003144

Altherr R, Soder CG (2018) Sapphirine as a breakdown product of garnet in a Variscan UHP/HT peridotite from the Vosges Mountains (France)—an indication of near-isothermal decompression. J Petrol 59:2221–2243. https://doi.org/10.1093/petrology/egy096

Altherr R, Henjes-Kunst F, Langer C, Otto J (1999) Interaction between crustal-derived felsic and mantle-derived mafic magmas in the Oberkirch Pluton (European Variscides, Schwarzwald, Germany). Contrib Mineral Petrol 137:304–322

Altherr R, Holl A, Hegner E, Langer C, Kreuzer H (2000) High-potassium, calc-alkaline I-type plutonism in the European Variscides: northern Vosges (France) and northern Schwarzwald (Germany). Lithos 50:51–73

Altherr R, Hanel M, Schwarz WH, Wimmenauer W (2019) Petrology and U-Pb zircon age of the Variscan porphyroclastic Rand Granite at the southeastern margin of the Central Schwarzwald Gneiss Complex (Germany). Int J Earth Sci 108:1879–1895. https://doi.org/10.1007/s00531-019-01738-2

An S-C, Li S-G, Liu Z (2018) Modification of the Sm-Nd isotopic system in garnet induced by retrogressive fluids. J Metamorph Geol 36:1039–1048. https://doi.org/10.1111/jmg.12426

Anderson ED, Moecher DP (2007) Omphacite breakdown reactions and relation to eclogite exhumation rates. Contrib Mineral Petrol 154:253–277. https://doi.org/10.1007/s00410-007-0192-x

Bach W, Peucker-Ehrenbrink B, Hart SR, Blusztajn JS (2003) Geochemistry of hydrothermally altered oceanic crust: DSDP/ODP Hole 504B—implications for seawater-crust exchange budgets and Sr- and Pb-isotopic evolution of the mantle. Geochem Geophys Geosyst 4:8904. https://doi.org/10.1029/2002GC000419

Bali E, Audétat A, Keppler H (2011) The mobility of U and Th in subduction zone fluids: an indicator of oxygen fugacity and fluid salinity. Contrib Mineral Petrol 161:597–613. https://doi.org/10.1007/s00410-010-0552-9

Barnes JD, Manning CE, Scambelluri M, Selverstone J (2018) The behaviour of Halogens during subduction-zone processes. In: Harlov DE, Aranovich L (eds) The Role of Halogens in Terrestrial and Extraterrestrial Geochemical Processes. Springer International Publishing AG, Berlin, pp 1–19 (**10.1007/978-3-642-28394-9**)

Benmammar A, Berger J, Triantafyllou A, Duchene S, Bendaoud A, Baele J-M, Bruguier O, Diot H (2020) Pressure-temperature conditions and significance of Upper Devonian eclogite and amphibolite facies metamorphisms in southern French Massif Central. Earth Sci Bull 191:28. https://doi.org/10.1051/bsgf/2020033

Berger J, Féménias O, Ohnenstetter D, Bruguier O, Plissart G, Mercier J-C, Demaiffe D (2010) New occurrence of UHP eclogites in Limousin (French Massif Central): Age, tectonic setting and fluid-rock interactions. Lithos 118:365–382. https://doi.org/10.1016/j.lithos.2010.05.013

Bons PD, Fusswinkel T, Gomez-Rivas E, Markl G, Wagner T, Walter B (2014) Fluid mixing from below in unconformity-related hydrothermal ore deposits. Geology 42:1035–1038. https://doi.org/10.1130/G35708.1

Brätz H, Klemd R (2002) Analyses of rare earth elements in geological samples by laser ablation - inductively coupled plasma mass spectrometry (LA-ICP-MS). Agilent ICP-MS J (13), Publication no. 5988–6305EN:1–6. www.agilent.com/chem/icpms

Brockamp O, Schlegel A, Wemmer K (2015) Complex hydrothermal alteration and illite K-Ar ages in Upper Visean molasse sediments and magmatic rocks of the Variscan Badenweiler-Lenzkirch suture zone, Black Forest, Germany. Int J Earth Sci 104:683–702. https://doi.org/10.1007/s00531-014-1118-2

Büsch W, Mehnert KR (1991) Antiperthites in granulites and similar structures in migmatites of the Black Forest. N Jahrb Mineral Abh 162:117–133

Büsch W, Hofer A, Spohn A (1985) Tholeiitische Amphibolite des Schwarzwaldes: eine Vergesellschaftung von MORB und IAT? N Jahrb Mineral Abh 152:23–44

Cabanis PB, Thiéblement D (1988) La discrimination des tholéiites continentals et des basalts arrière-arc. Proposition d'un nouveau diagramme, le triangle Th–3Tb–2Ta. Bull Soc Géol France 4:927–935

Chen F, Hegner E, Todt W (2000) Zircon ages and Nd isotopic and chemical compositions of orthogneisses from the Black Forest, Germany: evidence for a Cambrian magmatic arc. Int J Earth Sci 88:791–802

Chen F, Todt W, Hann HP (2003) Zircon and Garnet geochronology of eclogites from the Moldanubian Zone of the Black Forest, Germany. J Geol 111:207–222

de Hoÿm LM, Pitra P, Cagnard F, Le Bayon B (2020) Prograde and retrograde *P-T* evolution of a Variscan high-temperature eclogite, French Massif Central. Haut-Allier Earth Sci Bull 191:14

Eigenfeld-Mende I (1948) Metamorphe Umwandlungserscheinungen an Metabasiten des Südschwarzwaldes. Mitteilungen der Badische Geologischen Landesanstalt NF 1:1–111

Enami M, Zang Q, Yin Y (1993) High-pressure eclogites in northern Jiangsu—southern Shandong province, eastern China. J Metamorph Geol 11:589–603

Epp T, Walter BF, Scharrer M, Lehmann G, Henze K, Heimgärtner C, Bach W, Markl G (2019) Quartz veins with associated Sb-Pb-Ag±Au mineralization in the Schwarzwald, SW Germany: a record of metamorphic cooling, tectonic rifting, and element remobilization processes in the Variscan belt. Mineral Deposita 54:281–306. https://doi.org/10.1007/s00126-018-0855-8

Erdmannsdörffer OH (1938) Eklogit im Schwarzwald und seine retrograde Umwandlung. J Geol 46:438–447

Ernst WG, Liu J (1998) Experimental phase equilibrium study of Al- and Ti-contents of calcic amphibole in MORB—a semiquantitative thermobarometer. Am Mineral 83:952–969

Faryad SW, Jedlicka R, Collett S (2013) Eclogite facies rocks of the Monotonous unit, clue to Variscan suture in the Moldanubian Zone (Bohemian Massif). Lithos 179:353–363. https://doi.org/10.1016/j.lithos.2013.07.015

Finger F, Steyrer HP (1995) A tectonic model for the Eastern Variscides: Indications from a chemical study of amphibolites in the south-eastern Bohemian Massif. Geol Carpathica 46:127–150

Flöttmann T, Kleinschmidt G (1989) Structural and basement evolution in the Central Schwarzwald Gneiss Complex. In: Emmermann R, Wohlenberg J (eds) The German Continental Deep Drilling Program (KTB)—Site-selection Studies in the Oberpfalz and Schwarzwald. Springer-Verlag, Berlin , pp 265–275

Fluck P (1974) Etude géochimique des amphibolites de Sainte-Marie-aux-Mines: essai de characterisation du paléovolcanisme et mise en evidence d'un exemple de métasomatisme liée à la tectonique. Sci Géol Bull 27:285–308

Franke W, Cocks LRM, Torsvik TH (2017) The Paleozoic Variscan oceans revisted. Gondwana Res 48:257–284. https://doi.org/10.1016/j.gr.2017.03.005

Fuchs G (1976) Zur Entwicklung der Böhmischen Masse. Jahrb Geol Bundesanst 119:45–61

Gale A, Dalton CA, Langmuir CH, Su Y, Schilling J-G (2013) The mean composition of ocean ridge basalts. Geochem Geophys Geosyst 14:489–518. https://doi.org/10.1029/2012GC004334

Garbe-Schönberg CD (1993) Simultaneous determination of thirty-seven trace elements in twenty-eight international rock standards by ICP-MS. Geostand Geoanalyt Res 17:81–103

Gardien V, Lardeaux J-M, Ledru P, Allemand P, Guillot S (1997) Metamorphism during late orogenic extension: insights from the French Variscan belt. Bull Soc Géol France 168:271–286

Glodny J, Grauert B (2009) Evolution of a hydrothermal fluid-rock interaction system as recorded by Sr isotopes: a case study from the Schwarzwald, SW Germany. Mineral Petrol 95:163–178. https://doi.org/10.1007/s00710-008-0034-1

Godard G, Mabit J-L (1998) Peraluminous sapphirine formed during retrogression of a kyanite-bearing eclogite from Pays de Léon, Armorican Massif, France. Lithos 43:15–29

Griffen DT, Gosney TC, Phillips WR (1982) The chemical formula of natural staurolite. Am Mineral 67:292–297

Hanel M, Lippolt HJ, Kober B, Wimmenauer W (1993) Lower Carboniferous Granulites in the Schwarzwald Basement Near Hohengeroldseck (SW-Germany). Naturwissenschaften 80:25–28

Hanel M, Montenari M, Kalt A (1999) Determining sedimentation ages of high-grade metamorphic gneisses by their palynological record: a case study in the northern Schwarzwald (Variscan Belt, Germany). Int J Earth Sci 88:49–59

Hanus D, Büsch W, Willgallis A (1984) Über die Bildungsbedingungen einer Amphibolitvarietät vom Schauinsland (Schwarzwald). N Jahrb Mineral Abh 148:259–275

Hegner E, Chen F, Hann HP (2001) Chronology of basin closure and thrusting in the internal zone of the Variscan belt in the Schwarzwald, Germany: evidence from zircon ages, trace element geochemistry, and Nd isotopic data. Tectonophysics 332:169–184

Hernández-Uribe D, Palin RM (2019) A revised petrological model for subducted oceanic crust: Insights from phase equilibrium modelling. J Metamorph Geol 37:745–768. https://doi.org/10.1111/jmg.12483

Holland TJB (1979) Experimental determination of the reaction Paragonite = Jadeite + Kyanite + H_2O, and internally consistent thermodynamic data for part of the system Na_2O–Al_2O_3–SiO_2–H_2O, with applications to eclogites and blueschists. Contrib Mineral Petrol 68:293–301

Hyppolito T, Cambeses A, Angioboust S, Raimondo T, García-Casco A, Juliani C (2018) Rehydration of eclogites and garnet-replacement processes during exhumation in the amphibolite facies. Geol Soc London Spec Publ 478:217–239

Jarrard RD (2003) Subduction fluxes of water, carbon dioxide, chlorine, and potassium. Geochem Geophys Geosyst 4:8905. https://doi.org/10.1029/2002GC000392

Jedlicka R, Faryad SW, Hauzenberger C (2015) Prograde metamorphic history of UHP granulites from the Moldanubian Zone (Bohemian Massif) revealed by major element and Y + REE zoning in garnets. J Petrol 56:2069–2088. https://doi.org/10.1093/petrology/egv066

Kalt A, Altherr R (1996) Metamorphic evolution of garnet-spinel peridotites from the Variscan Schwarzwald (Germany). Int J Earth Sci 85:211–224

Kalt A, Grauert B, Baumann A (1994a) Rb-Sr and U-Pb isotope studies on migmatites from the Schwarzwald (Germany): constraints on isotopic resetting during Variscan high-temperature metamorphism. J Metamorph Geol 12:667–680

Kalt A, Hanel M, Schleicher H, Kramm U (1994b) Petrology and geochronology of eclogites from the Variscan Schwarzwald (F.R.G.). Contrib Mineral Petrol 115:287–302

Kalt A, Altherr R, Hanel M (1995) Contrasting P-T conditions recorded in ultramafic high-pressure rocks from the Variscan Schwarzwald (F.R.G.). Contrib Mineral Petrol 121:45–60

Kalt A, Altherr R, Hanel M (2000) The Variscan basement of the Schwarzwald. Berichte der Deutschen Mineralogischen Gesellschaft, Beiheft 2. Eur J Mineral 12:1–43

Kawamoto T, Mibe K, Bureau H, Reguer S, Mocuta C, Kubsky S, Thiaudière D, Ono S, Kogiso T (2014) Large-ion lithophile elements delivered by saline fluids to the sub-arc mantle. Earth Planets Space 66:61

Kelley KA, Plank T, Ludden J, Staudigel H (2003) Composition of altered oceanic crust at ODP Sites 801 and 1149. Geochem Geophys Geosyst 4:8910. https://doi.org/10.1029/2002GC000435

Keppler H (2017) Fluids and trace element transport in subduction zones. Am Mineral 102:5–20. https://doi.org/10.2138/am-2017-5716

Kessel R, Schmidt MW, Ulmer P, Pettke T (2005a) Trace element signature of subduction-zone fluids, melts and supercritical liquids at 120–180 km depth. Nature 437:724–727. https://doi.org/10.1038/nature03971

Kessel R, Ulmer P, Pettke T, Schmidt MW, Thompson AB (2005b) The water-basalt system at 4 to 6 GPa: phase relations and second critical endpoint in a K-free eclogite at 700 to 1400 °C. Earth Planet Sci Lett 237:873–892. https://doi.org/10.1016/j.epsl.2005.06.018

Klein H, Wimmenauer W (1984) Eclogites and their retrograde transformation in the Schwarzwald (Fed. Rep. Germany). N Jahrb Mineral Mh 1984:25–38

Klemd R (2013) Metasomatism during high-pressure metamorphism: eclogites and blueschist-facies rocks. In: Harlov DE, Austrheim H (eds) Metasomatism and the chemical transformation of rock. Lecture Notes in Earth System Sciences, Springer, Berlin, pp 351–413

Kober B, Kalt A, Hanel M, Pidgeon RT (2004) SHRIMP dating of zircons from high-grade metasediments of the Schwarzwald/SW-Germany and implications for the evolution of the Moldanubian basement. Contrib Mineral Petrol 147:330–345. https://doi.org/10.1007/s00410-004-0560-8

Kossmat F (1927) Gliederung des variszischen Gebirgsbaues. Abhandlungen des Sächsischen Geologischen Landesamtes 1:1–39

Lardeaux JM, Ledru P, Daniel I, Duchene S (2001) The Variscan French Massif Central—a new addition to the ultra-high pressure metamorphic 'club': exhumation process and geodynamic consequences. Tectonophysics 332:143–167

Le Maitre RW (2002) Igneous rocks—a classification and glossary of terms, 2nd edn. Cambridge University Press, Cambridge, p 236

Lentz DR (1998) Petrogenetic evolution of felsic volcanic sequences associated with Phanerozoic volcanic-hosted massive sulphide systems: the role of extensional geodynamics. Ore Geol Rev 12:289–327

Lippolt HJ, Kirsch H (1994) Isotopic investigation of post-Variscan plagioclase sericitization in the Schwarzwald Gneiss Massif. Chem Erde 54:179–198

Lotout C, Poujol M, Pitra P, Anczkiewicz R, Van Den Driessche J (2020) From burial to exhumation: emplacement and metamorphism of mafic eclogitic terranes constrained through multimethod petrochronology, case study from the Lévézou Massif (French Massif Central, Variscan Belt). J Petrol 61:1–27. https://doi.org/10.1093/petrology/egaa046

Marschall HR, Kalt A, Hanel M (2003) Evolution of a Variscan lower-crustal segment: a study of granulites from the Schwarzwald, Germany. J Petrol 44:227–253

McDonough WF, Sun S-S (1995) The composition of the Earth. Chem Geol 120:223–253

Mehnert KR, Büsch W (1982) The initial stage of migmatite formation. N Jahrb Mineral Abh 145:211–238

Mibe K, Kawamoto T, Matsukage KN, Fei Y, Ono S (2011) Slab melting versus slab dehydration in subduction-zone magmatism. PNAS 108:8177–8182. https://doi.org/10.1073/pnas.1010968108

Miyashiro A (1975) Volcanic rock series and tectonic setting. Ann Rev Earth Planet Sci 3:251–269

Naemura K, Ikuta D, Kagi H, Odake S, Ueda T, Ohi S, Kobayashi T, Svojtka M, Hirajima T (2011) Diamond and other possible ultradeep evidence discovered in the orogenic spinel-garnet peridotite from the Moldanubian Zone of the Bohemian Massif, Czech Republic. In: Dobrzhinetskaya LF, Faryad SW, Wallis S, Cuthbert S (eds) Ultrahigh-Pressure Metamorphism. Elsevier, Amsterdam, pp 77–111 (**10.1016/B978-0-12-385144-4.00002-3**)

Nakamura D (2002) Kinetics of decompressional reactions in eclogitic rocks—formation of plagioclase coronas around kyanite. J Metamorph Geol 20:325–333

Pearce JA (1982) Trace element characteristics of lavas from destructive plate boundaries. In: Thorpe RS (ed) Andesites. John Wiley and Sons, Hoboken, pp 525–548

Pearce JA, Gale GH (1977) Identification of ore-deposition environment from trace-element geochemistry of associated igneous host rocks. Geol Soc London Spec Publ 7:14–24

Pearce JA, Perkins WT, Westgate JA, Gorton MP, Jackson SE, Neal CR, Chenery SP (1997) A compilation of new and published major and trace element data for NIST SRM 610 and NIST SRM 612 glass reference materials. Geostand Geoanalyt Res 21:115–144

Penniston-Dorland SC, Kohn MJ, Manning CE (2015) The global range of subduction zone thermal structures from exhumed blueschists and eclogites: Rocks are hotter than models. Earth Planet Sci Lett 428:243–254. https://doi.org/10.1016/j.epsl.2015.07.031

Perraki M, Faryad SW (2014) First finding of microdiamond, coesite and other UHP phases in felsic granulites in the Moldanubian Zone: Implications for deep subduction and a revised geodynamic model for Variscan orogeny in the Bohemian Massif. Lithos 202–203:157–166. https://doi.org/10.1016/j.lithos.2014.05.025

Plank T (2005) Constraints from Thorium/Lanthanum on sediment recycling at subduction zones and the evolution of the continents. J Petrol 46:921–944. https://doi.org/10.1093/petrology/egi005

Plümper O, John T, Podladchikov YY, Vrijmoed JC, Scambelluri M (2017) Fluid escape from subduction zones controlled by channel-forming reactive porosity. Nat Geosci 10:150–156. https://doi.org/10.1038/NGEO2865

Pouchou JL, Pichoir F (1984) A new model for quantitative analyses. I. Application to the analysis of homogeneous samples. La Recherche Aérospatiale 3:13–38

Pouchou JL, Pichoir F (1985) "PAP" φ(ρZ) correction procedure for improved quantitative microanalysis. In: Armstrong JT (ed) Microbeam analysis. San Francisco Press, San Francisco, pp 104–106

Rebay G, Powell R, Diener JFA (2010) Calculated phase equilibria for a MORB composition in a P-T range, 450–650 °C and 18–28 kbar: the stability of eclogite. J Metamorph Geol 28:635–645. https://doi.org/10.1111/j.1525-1314.2010.00882.x

Rey P, Burg J-P, Caron J-M (1992) Middle and Late Carboniferous extension in the Variscan Belt: structural and petrological evidences from the Vosges massif (Eastern France). Geodin Acta 5:17–36

Ross P-S, Bédard JH (2009) Magmatic affinity of modern and ancient subalkaline volcanic rocks determined from trace-element discriminant diagrams. Can J Earth Sci 46:823–839. https://doi.org/10.1139/E09-054

Rustioni G, Audétat A, Keppler H (2019) Experimental evidence for fluid-induced melting in subduction zones. Geochem Persp Lett 11:49–54. https://doi.org/10.7185/geochemlet.1925

Săbău G, Alberico A, Negulescu E (2002) Peraluminous sapphirine in retrogressed kyanite-bearing eclogites from the South Carpathians: Status and implications. Int Geol Rev 44:859–876

Saunders AD, Norry MJ, Tarney J (1988) Origin of MORB and chemically depleted mantle reservoirs: trace element constraints. J Petrol. https://doi.org/10.1093/petrology/Special_Volume.1.415

Schaltegger U (2000) U-Pb geochronology of the Southern Black Forest Batholith (Central Variscan Belt): timing of exhumation and granite emplacement. Int J Earth Sci 88:814–828

Scherer EE, Mezger K, Münker C (2002) Lu-Hf ages of high-pressure metamorphism in the Variscan fold belt of southern Germany. Geochim Cosmochim Acta 66(Supplement 1):A677

Schmidt MW, Jagoutz O (2017) The global systematics of primitive arc melts. Geochem, Geophys Geosyst 18:2817–2854. https://doi.org/10.1002/2016GC006699

Schramm B, Devey CW, Gillis KM, Lackschewitz K (2005) Quantitative assessment of chemical and mineralogical changes due to progressive low-temperature alteration of East Pacific Rise basalts from 0 to 9 Ma. Chem Geol 218:281–313. https://doi.org/10.1016/j.chemgeo.2005.01.011

Sebert M, Wimmenauer W (1992) Metagabbros and meta-anorthosites in the Southern Black Forest (Germany)—fragments of an ancient layered intrusion? Jahreshefte des Geologischen Landesamtes Baden-Württemberg 34:193–212

Seifert F (1974) Stability of sapphirine: a study of the aluminous part of the system MgO-Al_2O_3-SiO_2-H_2O. J Geol 82:173–204

Sorger D, Hauzenberger CA, Finger F, Linner M (2020) Two generations of Variscan garnet: Implications from a petrochronological study of a high-grade Avalonia-derived paragneiss from the Drosendorf unit, Bohemian Massif. Gondwana Res 85:124–148. https://doi.org/10.1016/j.gr.202004.004

Staudigel H (2014) Chemical fluxes from hydrothermal alteration of the oceanic crust. In: Holland HD, Turekian KK (eds) Treatise on Geochemistry, 2nd edn. Elsevier, Amsterdam, pp 583–606

Staudigel H, Plank T, White B, Schmincke HU (1996) Geochemical fluxes during seafloor alteration of the basaltic upper oceanic crust: DSDP Sites 417 and 418. Am Geophys Union Geophys Monogr Series 96:19–38

Suter H (1924) Petrographie des Grundgebirges von Laufenburg und Umgebung (Südschwarzwald). Schweiz Mineral Petrogr Mitt 4:89–336

Thiele O (1984) Zum Deckenbau und Achsenplan des Moldanubikums der Südlichen Böhmischen Masse (Österreich). Jahrb Geol Bundesanst 126:513–523

Thiéry V, Rolin P, Dubois M, Caumon M-C (2015) Discovery of metamorphic microdiamonds from the parautochthonous units of the Variscan French Massif Central. Gondwana Res 28:954–960. https://doi.org/10.1016/j.gr.2015.05.009

Todt WA, Büsch W (1981) U-Pb investigations on zircons from pre-Variscan gneisses—A study from the Schwarzwald, West Germany. Geochim Cosmochim Acta 45:1789–1801

Tsay A, Zajacz Z, Sanchez-Valle C (2014) Efficient mobilization and fractionation of rare-earth elements by aqueous fluids upon slab dehydration. Earth Planet Sci Lett 398:101–112. https://doi.org/10.1016/j.epsl.2014.04.042

Tsay A, Zajacz Z, Ulmer P, Sanchez-Valle C (2017) Mobility of major and trace elements in the eclogite-fluid system and element fluxes upon slab dehydration. Geochim Cosmochim Acta 198:70–91. https://doi.org/10.1016/j.gca.2016.10.038

Ulmer P, Trommsdorff V (1995) Serpentine stability to mantle depths and subduction-related magmatism. Science 268:858–861

Vanderhaeghe O, Laurent O, Gardien V, Moyen J-F, Gébelin A, Chelle-Michou C, Couzinié S, Villaros A, Bellanger M (2020) Flow of partially molten crust controlling construction, growth and collapse of the Variscan orogenic belt: the geologic record of the French Massif Central. BSGF Earth Sci Bull 191:25. https://doi.org/10.1051/bsgf/2020013

Wang Y, Prelević D, Foley SF (2019) Geochemical characteristics of lawsonite blueschists in tectonic mélange from the Tavşanlı Zone, Turkey: potential constraints on the origin of Mediterranean potassium-rich magmatism. Am Mineral 104:724–743. https://doi.org/10.2138/am-2019-6818

Wei CJ, Clarke GL (2011) Calculated phase equilibria for MORB compositions: a reappraisal of the metamorphic evolution of lawsonite eclogite. J Metamorph Geol 29:939–952. https://doi.org/10.1111/j.1525-1314.2011.00948.x

Wei CJ, Duan ZZ (2019) Phase relations in metabasic rocks: constraints from the results of experiments, phase modelling and ACF analysis. Geol Soc London Spec Publ 474:25–45

Weyer S, Jarick J, Mezger K (1999) Quantitative temperature-time information from retrograde diffusion zoning in garnet: constraints for the *P-T-t* history of the Central Black Forest, Germany. J Metamorph Geol 17:449–461

Whitney DL, Evans BW (2010) Abbreviations for names of rock-forming minerals. Am Mineral 95:185–187. https://doi.org/10.2138/am.2010.3371

Wickert F, Altherr R, Deutsch M (1990) Polyphase Variscan tectonics and metamorphism along a segment of the Saxothuringian-Moldanubian boundary: The Baden-Baden Zone, northern Schwarzwald (F.R.G.). Int J Earth Sci 79:627–647

Will TM, Schmädicke E (2001) A first find of retrogressed eclogites in the Odenwald Crystalline Complex, Mid-German Crystalline Rise, Germany: evidence for a so far unrecognised high-pressure metamorphism in the Central Variscides. Lithos 59:109–125

Wimmenauer W (1984) Das prävariskische Kristallin im Schwarzwald. Fortschritte der Mineralogie 62. Beiheft 2:69–86

Wimmenauer W (1988) Precambrian in the Horst Mountains of the Rhine Graben Area. In: Zoubek V (ed) Precambrian in Younger Fold Belts. Wiley and Sons, New York, pp 381–408

Wimmenauer W, Lim SK (1988) L'association leptyno-amphibolique de la Forêt-Noire (R.F.A.). Bull Soc géol France. https://doi.org/10.2113/gssgfbull.IV.1.35

Winchester JA, Floyd PA (1976) Geochemical magma type discrimination—Application to altered and metamorphosed basic igneous rocks. Earth Planet Sci Lett 28:459–469

Winchester JA, Floyd PA (1977) Geochemical discrimination of different magma series and their differentiation products using immobile elements. Chem Geol 20:325–343

Wood DA (1980) The application of a Th-Hf-Ta diagram to problems of tectonomagmatic classification and to establishing the nature of crustal contamination of basaltic lavas of the British Tertiary volcanic province. Earth Planet Sci Lett 50:11–30

Xia K, Li X (2019) Basalt geochemistry as a diagnostic indicator of tectonic setting. Gondwana Res 65:43–67

Zack T, John T (2007) An evaluation of reactive fluid flow and trace element mobility in subducting slabs. Chem Geol 239:199–216. https://doi.org/10.1016/j.chemgeo.2006.10.020

Zack T, Moraes R, Kronz A (2004) Temperature dependence of Zr in rutile: empirical calibration of a rutile thermometer. Contrib Mineral Petrol 148:471–488. https://doi.org/10.1007/s00410-004-0617-8